International Journal of Innovative
Computing, Information and Control
Volume **19**, Number **4**, August **2023**

ICIC International ©2023 ISSN 1349-4198
pp. **1023–1055**

OPTIMAL PATH PLANNING METHOD FOR UAV BASED ON THE TANGENT POINT ALGORITHM IN URBAN ENVIRONMENT

Yuanlong Yue*, Daifeng Zhang, Lvyin Niu and Xin Zuo

Department of Automation
College of Information Science and Engineering
China University of Petroleum (Beijing)
No. 18, Fuxue Road, Changping District, Beijing 102249, P. R China
18401303505@163.com; 2238999354@qq.com; zuox@cup.edu.cn
*Corresponding author: yueyuanlong@cup.edu.cn

Received November 2022; revised February 2023

Abstract. *The UAV (unmanned aerial vehicle) has to bypass flight due to the complex distribution of obstacles in the urban environment. This paper proposes the TPA (tangent point algorithm) used in optimal path planning which can enable UAV to effectively avoid obstacles and achieve optimal flight metrics. Firstly, the environment model is established and the obstacles are reconstructed as two-dimensional circles. And the finite path is traversed and the optimal path is selected. Secondly, the UAV kinematic model is established to optimize the UAV flight mode and determine the flight strategy according to the adjacent obstacle circle. Thirdly, the UAV energy consumption model is established based on the energy transfer process and multi-stage optimal path. Finally, the simulation method is used to compare the optimal paths of TPA, A* (A-Star), PRM (probabilistic road map), and RRT (rapidly-exploring random tree). TPA has the shortest calculation time and the collision-free optimal path. And the optimal power is chosen to ensure the bi-objective optimization of the flight time and energy consumption. The structural parameters of the UAV and the obstacle information are integrated to determine the optimal flight strategy of the UAV on the optimal path.*

Keywords: Bi-objective optimization, Circular common tangent, Flight strategy, Obstacle avoidance, Path planning, UAV

1. **Introduction.** Since the 1990s, UAV has come into the public view from the military field and is widely used in various fields [1,2], such as vegetation protection [3], emergency rescue [4], target reconnaissance [5], and cargo delivery [6], where path planning is the essential factor to achieve autonomous control of UAV. At present, how to achieve the optimal path for UAV in complex environments with intensive obstacles is still a hot research topic, which includes the collision-free optimal path and optimal flight strategy.

In recent years, researchers have proposed numerous collision-free path generation methods in path planning, which are mainly divided into the graph-based algorithm, sampling-based algorithm, and intelligent optimization algorithm.

The graph-based algorithms are mainly composed of the A*, visual graph [7], and tangent methods [8]. The A* algorithm plans the path by constructing a cost function, which is a typical depth-first pathfinding algorithm. František et al. introduced the Basic Theta*, Phi*, RSR (rectangular symmetry reduction), and JPS (jump point search) which are the improved A* algorithm based on the path planning requirements of mobile robots and compared the characteristics of these four algorithms in different environments [9].

DOI: 10.24507/ijicic.19.04.1023

The JPS is suitable for the computational speed-first scenario and the Basic Theta* algorithm performs well for the path length-first scenario. In terms of the convergence time of traditional A* algorithm being too long to meet the demand, Saeid et al. proposed an innovative algorithm that mixes A* search engine and visibility diagram planning. And this algorithm is used to find the shortest non-holonomic path in a continuous-discrete environment [10].

The visual diagram and tangent algorithms based on obstacle information are more efficient and have shorter computational time for pathfinding [11-13]. The visual diagram algorithm was first proposed by Tomás and Michael [14]. The algorithm finds an obstacle by continuously scanning the map and determines whether the UAV is collided with obstacle. Doyle and Jones early proposed the tangent algorithm [15], which simplifies the pathfinding problem to one of connecting the starting and ending points to a road network to obtain the best path, where the road network consists of a common tangent among each of obstacles.

An autonomous path planning algorithm based on tangent intersection and target guidance strategy was proposed by Liu et al. [16]. The algorithm generates two sub-paths by elliptic tangent method, which is selected according to four heuristic rules. Then the path point is obtained through connecting the sub-paths with the tangent intersection, and the algorithm uses a three times B spline curve to smooth the path points to generate the optimal path. However, the authors did not consider the inner tangent of the obstacle ellipse, and the UAV paths selected are easy to fall into local optimum. A tangent-based collision prediction and avoidance algorithm was discussed by Ossyra et al. [17]. Meanwhile, the authors considered a velocity-dependent ellipsoidal geometry to avoid high-density ADS-B traffic areas. However, the algorithm did not refer to the smooth path and UAV turning radius when generating waypoints.

The PRM and RRT are the typical sampling-based algorithms. The PRM forms a road network by randomly picking points to get the optimal path [18,19]. In the navigation field, Li et al. proposed an improved PRM to solve the path planning problem in the area without road network [20]. Instead of random sampling, it uses non-uniform sampling based on a greedy algorithm. Also, it can obviously improve the computational efficiency and the quality of the generated paths. Huppi et al. proposed a real-time algorithm for Temporal-PRM [21], which considers the temporal availability of nodes. It can meet the dynamic characteristics of UAV pathfinding requirements due to the certain dynamic obstacle avoidance roles. Uzun et al. proposed a hybrid algorithm combining the A* and PRM [22].

The RRT is applied in path planning through random spanning trees [23-27]. Wang et al. proposed a Neural-RRT* to improve the sampling process using the non-uniform sampling method [28]. First, the algorithm uses the A* to obtain a training set of optimal paths, which is used to train the sampling process of the CNN network and performs sampling based the trained sampling model and effectively improves the quality and computational efficiency of the generated paths. Qi et al. proposed an improved algorithm of MOD-RRT* based on prior knowledge for robot navigation in unknown dynamic environments [29]. The algorithm uses the RRT to generate the state tree as prior knowledge used to optimize the generated paths. In particular, the algorithm can quickly adjust and generate a high-quality path using the prior knowledge when pop-up obstacles appear in the path.

Intelligent optimization algorithms are divided into artificial intelligence and bionic intelligence algorithms [30-32]. Intelligent optimization algorithm includes the Q-learning algorithm [33], machine learning (ML) algorithm [34], etc. The bionic intelligence algorithm

mainly consists of particle swarm optimization (PSO) [35], genetic algorithm (GA) [36], ant colony optimization (ACO) [37], and gray wolf optimization (GWO) [38].

2. **Summary.** From the above literature, it can be found that 1) The graph-based methods are more time-consuming when traversing all sub-paths, and the contrast is more obvious in complex environments; 2) The sampling-based algorithm achieves the balance between time efficiency and path quality, but still fails to meet the requirements of optimal paths, and meanwhile, the computing time performs steadily while the quality of paths generated varies each time; 3) The intelligent algorithm can generate satisfactory optimal paths of the condition that the computing time requirement is not high, and the cost that the computing efficiency of the intelligent algorithm is far from satisfactory even after optimization.

In order to efficiently plan collision-free paths in the static environment, this paper proposes an optimal path-planning method based on the viewable tangent point algorithm (TPA). Guided by the ending point, the path begins from the starting point and bypasses the obstacles based on the circle's tangent map. The sub-paths consist of common tangents connecting adjacent obstacle circles. The TPA can generate the shortest collision-free path by means of combining the arcs between tangent points of the same obstacle circle and comparing the lengths of different paths from the starting point to the ending point. The flight strategy is determined according to the UAV kinematic model. Synthetically, the optimal power and flight strategy are determined by integrating the multi-segment optimal path and the location information of the UAV and obstacle to ensure the optimal flight time and energy consumption of the UAV based on the optimal path.

The main contributions of this paper are as follows.

1) A new viewable path planning algorithm TPA is proposed. The building is reconstructed into a circle in a static environment, and the starting and ending points are fictitiously constructed as circles with radius of 0. There is a scope to select the obstacle circle near the start-end line. And the straight-line segment between the tangent points of two circles and the circular arc between the tangent points on the same circle are combined with different paths. The shortest path is selected as the optimal one by calculating the comparative path length. It is worth noting that the architectural reconstruction considers the safety distance between the UAV and the obstacle, that is, the UAV is able to fly along the round edge of the circular obstacle. The UAV also can avoid the smooth curve function construction of the path turning point because of the arc between the tangent points on the same circle as the UAV turning path.

2) The optimal path is combined with multiple straight-lines and arc segments. The speed and power of the UAV in the arc segment are only related to the radius of the obstacle circle. Therefore, the flight time of the UAV in the arc segment is independent of the flight strategy. In the linear segment, the different UAV flight strategies are proposed to guarantee the shortest flight time according to the length of the linear segment and the distribution of the different obstacle circles, which provides the theoretical principle for the bi-objective optimization of UAV flight time and energy consumption.

3) The TPA not only generates the shortest collision-free optimal path but also consumes the least computing time compared to the four algorithms in different complexity environments. Numerical simulation of the acceleration process and deceleration process of UAV kinematics proves the existence of an optimal solution for the time-energy consumption of the UAV acceleration and deceleration process by the weight method. And the optimal power is determined by selecting the appropriate weight parameters. The optimal path, flight strategy, and optimal power of the UAV are integrated to determine

the optimal flight strategy of the UAV and ensure the bi-objective optimization of the UAV flight time and energy consumption.

The other chapters of this paper are organized as follows. In Section 3, the interesting problem is stated and the system model is presented. In Section 4, the proposed path planning algorithm and flight strategy are analyzed. Section 5 provides computer simulation experiments to validate the proposed approach. Finally, conclusions are drawn in Section 6.

The definitions and descriptions of the variables used in this paper are shown in Table 1.

Table 1. Symbols and meanings

Symbol	Meaning
S	The position of start-point
E	The position of end-point
P_i	Circles of obstacle
S_{su}	Acceleration distance of UAV
S_{sd}	Deceleration distance of UAV
t_{su}	Acceleration time of UAV
t_{sd}	Deceleration time of UAV
Ob	A set of two-dimensional arrays is used to store the parameters of all obstacle circles
PC	A set of two-dimensional arrays is used to store the parameters of the shortest path circles
TP	A set of three-dimensional arrays is used to store the information about all common tangent points
Nm	A set of two-dimensional arrays is used to store the serial numbers of all paths
RN	A set of one-dimensional arrays is used to store the number of paths between two obstacle circles
BR	A set of two-dimensional arrays is used to store the information about the tangent points of the shortest path
UAV	Unmanned aerial vehicle
TPA	Tangent point algorithm
PRM	Probabilistic road map
RRT	Rapidly-exploring random tree

3. **Problem Statement.** There are lots of tall buildings crisscrossing in the urban environment, and the UAV needs to fly normally and perform tasks in this complex environment. The three-dimensional scenario of the UAV performing the mission is shown in Figure 1. The UAV needs to reach E from S. Since there may be many buildings as obstacles during the flight, the UAV not only needs to avoid these obstacles with the optimal path to reach the designated location for standing by but also needs to consider the flight strategy to ensure the optimal flight time and energy consumption. In this paper, the path planning algorithm only considers the scenario where the obstacle height is higher than the normal flight height of the UAV. The UAV adopts the obstacle avoidance method of maintaining the flight height and bypassing around the obstacle horizontally in order to reduce the optimal path computational time and narrow the path search space.

FIGURE 1. Three-dimensional scenario of UAV performing tasks

In fact, in addition to the horizontal bypassing obstacle avoidance method, the UAV can also adopt the spanning obstacle avoidance method and the combined bypassing and spanning obstacle avoidance method in three-dimensional space. The latter two obstacles avoidance methods need to consider the relationship between UAV flight height and obstacle height. Then the different obstacle avoidance methods are determined based on the measurement of the UAV flight time and energy consumption in different situations. This paper focuses on the obstacle avoidance method in the urban environment where the obstacle is higher than the UAV flight height and takes a bypass flight.

Therefore, the three-dimensional scenario is projected onto the ground to form a two-dimensional scenario in the case of facilitating the subsequent operation of path planning, as shown in Figure 2. It is reasonable that we focus on two-dimensional scenarios from the planning level while three-dimensional scenarios would be considered from the operational level.

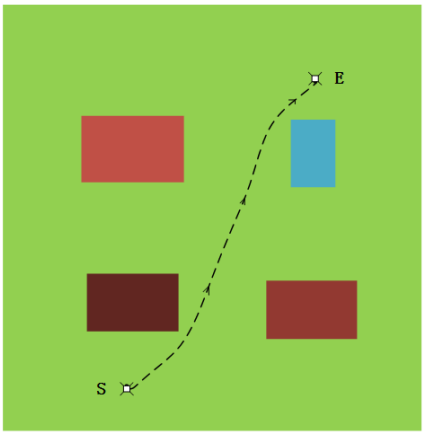

FIGURE 2. Two-dimensional scenario of UAV performing tasks

The visual graph method transforms the UAV path planning problem into searching for the shortest line segment set between the starting point and the target point. It is easy to collide with obstacles and the generated path is not smooth enough and since the shortest path searched is a line segment connecting the vertices of obstacles. The path searched takes longer when the amounts of environmental obstacles and feature information are large. Tangent maps are constructed with tangent lines from the source to the visible vertices on polygonal obstacles, and this process requires complex mathematical calculations and takes more time.

Buildings in the urban environment are mainly polygons, such as squares, rectangles, and triangles. Polygons are not uniform in shape, and direct planning of UAV flight path will lead to the above problems. Therefore, a uniform reconstruction of buildings is required in UAV path planning. In order to overcome the abovementioned shortcomings, obstacles are uniformly modeled as ellipses, which can describe various obstacles and facilitate subsequent path planning operations [14]. For simplicity, [11] assumes that each polygonal shape obstacle is surrounded by a virtual circle with all its vertices inside this circle. This process is done by using the randomized incremental algorithm. This algorithm determines the smallest enclosing circle surrounding the vertices of a given polygon.

There will always be blank areas in the reconstructed graphics whether the buildings are reconstructed into ellipses or circles, such as rectangles reconstructed into circles or squares reconstructed into ellipses. However, for better model building, path planning, algorithm implementation, saving more flight time and flight energy consumption of UAVs, and avoiding collisions between UAVs and obstacles, such reconstructed operations are acceptable and understandable. At the same time, the reconstructed circle is able to avoid trap obstacles. And the UAV considering the safety distance is able to fly along the round edge of the circular obstacles, which not only avoids the construction of smooth curve functions at the UAV path turning points but also can avoid the maze environment composed of circular obstacles.

As shown in Figure 3, four shapes of obstacles are shown, and the dashed circles constructed are the outer circles of the polygons. The solid line circle constructed is the shape of the polygonal obstacles after reconstruction because of the safe distance between the UAV and the obstacles. Then the UAV can keep a safe distance from the obstacles while ensuring flight on the round side. And the solid line circle can describe various obstacles to facilitate subsequent path planning operations. The obstacles for the UAV to perform its task are shown in Figure 4 after architectural reconstruction.

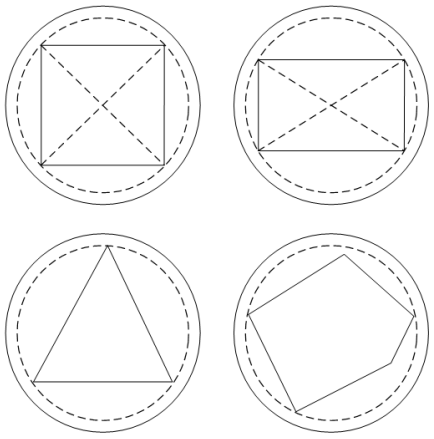

FIGURE 3. Architectural reconstruction

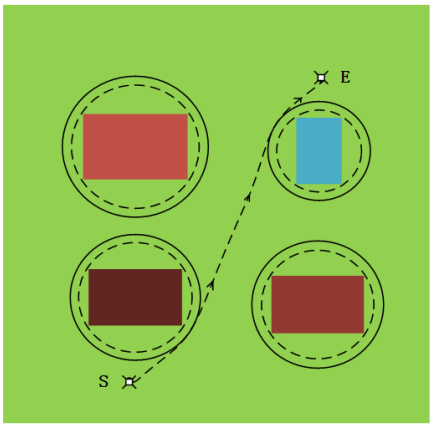

FIGURE 4. Two-dimensional scenario of architectural reconstruction

3.1. **Environmental model.** The safe distance r_{safe} that the UAV needs to maintain from the obstacle during obstacle reconstruction consists of two parts, where l_{stop} is the braking distance from the maximum speed to the horizontal standstill when the UAV encounters an emergency, and $l_{uav}/2$ is half of the longest distance of the UAV itself, i.e., the safety distance should satisfy the following equation.

$$r_{safe} = l_{stop} + \frac{l_{uav}}{2} \tag{1}$$

In two dimensions, it is supposed that the coordinate of the circle center of the obstacle circle O_i is (x_i, y_i) and the radius is r_i which includes r_{safe} to conveniently denote. At the same time, the coordinate of the circle center of the obstacle circle O_j $(j \neq i)$ is (x_j, y_j) and the radius is r_j. The equation of the common tangent of two circles is $y = k_{ct}x + b_{ct}$, and then the slope and b values of the four common tangents should satisfy the following equations.

$$\begin{cases} k_{ct_{1,2}} = \dfrac{(x_i - x_j)(y_i - y_j) \pm |r_i - r_j| \sqrt{(x_i - x_j)^2 + (y_i - y_j)^2 - (r_i - r_j)^2}}{(x_i - x_j)^2 - (r_i - r_j)^2} \\ b_{ct_{1,2}} = \dfrac{(x_i r_j - x_j r_i) k_{ct_{1,2}} + (y_j r_i - y_i r_j)}{r_i - r_j} \end{cases} \tag{2}$$

$$\begin{cases} k_{ct_{3,4}} = \dfrac{(x_i - x_j)(y_i - y_j) \pm (r_i + r_j) \sqrt{(x_i - x_j)^2 + (y_i - y_j)^2 - (r_i + r_j)^2}}{(x_i - x_j)^2 - (r_i + r_j)^2} \\ b_{ct_{3,4}} = \dfrac{-(x_i r_j + x_j r_i) k_{ct_{3,4}} + (y_j r_i + y_i r_j)}{r_i + r_j} \end{cases} \tag{3}$$

The coordinates of the tangent points of the four common tangents at the two circles are $A\left(x_{i\text{-}ctp}, y_{i\text{-}ctp}\right)$ and $B\left(x_{j\text{-}ctp}, y_{j\text{-}ctp}\right)$, satisfying the following equations.

$$A\left(x_{i\text{-}ctp}, y_{i\text{-}ctp}\right) = \left(\frac{x_i - k_{ct}\left(b_{ct} - y_i\right)}{k_{ct}^2 + 1}, \frac{\left(k_{ct}x_i + b_{ct} - y_i\right)^2 - \left(k_{ct}^2 + 1\right) r_i^2}{k_{ct}^2 + 1} \right) \tag{4}$$

$$B\left(x_{j\text{-}ctp}, y_{j\text{-}ctp}\right) = \left(\frac{x_j - k_{ct}\left(b_{ct} - y_j\right)}{k_{ct}^2 + 1}, \frac{\left(k_{ct}x_j + b_{ct} - y_j\right)^2 - \left(k_{ct}^2 + 1\right) r_j^2}{k_{ct}^2 + 1} \right) \tag{5}$$

Especially, it is assumed that the coordinate of the circle center of the starting point is (x_s, y_s) and the radius is 0. Also, the coordinate of the circle center of the ending point is (x_E, y_E) and the radius is 0. There are equations of the tangent line and coordinates of the tangent point between the start-end points of the UAV and the adjacent circle according to Equations (2)-(5).

3.2. **Kinematic model.** The UAV in urban environment arrives at the destination E from the departure place S. The process of UAV performing the mission mainly consists of accelerated flight process, uniform flight process and decelerated flight process, and the following is the kinematic modeling of the three motion processes.

1) **UAV acceleration model**

Theorem 3.1. *It is assumed that the UAV accelerates from 0 to the maximum speed $v_{\max}$ with constant acceleration power P_{su} and the UAV is subjected to the air resistance $f = kv^2$ in this process, then the UAV acceleration distance S_{su} and acceleration time t_{su} satisfy the following equations.*

$$S_{su} = \frac{m}{3k} \ln \left(\frac{P_{su}}{P_{su} - kv_{\max}^3} \right) \tag{6}$$

$$t_{su} = \frac{1}{3} P_{su}^{-\frac{1}{3}} k^{-\frac{2}{3}} m \left[\frac{1}{2} \ln \left(1 + \frac{3y}{(y-1)^2} \right) - \sqrt{3} \arctan \left(\frac{\sqrt{3}y}{y+2} \right) \right] \tag{7}$$

where $y = \sqrt[3]{\frac{k}{P_{su}}} v_{\max}$.

Firstly, it is necessary to analyze the force of the UAV acceleration process. According to the Newton's second law, the force equation is obtained. The equation needs to be decomposed and transformed to obtain a new equation. The equation is indefinitely integrated to obtain a new equation again. According to the changing rules of the acceleration process speed, the acceleration time formula (7) is obtained. At the same time, the indirect method combined with integration is used to solve the accelerated distance formula because the distance formula cannot be solved directly by integration. Through a series of formula derivation and substitution of related formulas, the acceleration distance formula (6) is finally obtained.

2) **UAV deceleration model**

Theorem 3.2. *It is assumed that the UAV decelerates from the maximum speed $v_{\max}$ to 0 with constant deceleration power P_{sd} and the UAV is subjected to the air resistance $f = kv^2$ in this process, then the UAV deceleration distance S_{sd} and deceleration time t_{sd} satisfy the following equations.*

$$S_{sd} = \frac{m}{3k} \ln \left(\frac{kv_{\max}^3}{P_{sd}} + 1 \right) \tag{8}$$

$$t_{sd} = \frac{1}{3} P_{sd}^{-\frac{1}{3}} k^{-\frac{2}{3}} m \left[\frac{1}{2} \ln \left(1 - \frac{3x}{(x+1)^2} \right) + \sqrt{3} \arctan \left(\frac{\sqrt{3}x}{2-x} \right) \right] \tag{9}$$

where $x = \sqrt[3]{\frac{k}{P_{sd}}} v_{\max}$.

The formula derivation principle of UAV deceleration process is the same as that of acceleration process, which is no longer described.

3) **UAV homogeneous model**

It is supposed that there are any two points $C(x_1, y_1)$ and $D(x_2, y_2)$ on the circle of the obstacle circle O_i. Then the arc lengths of the two points on the circle satisfy the following equation.

$$\widehat{CD} = \pi r_i \frac{\arcsin \frac{|CD|}{2r_i}}{90^\circ} \tag{10}$$

where $|CD| = \sqrt{(x_1 - x_2)^2 + (y_1 - y_2)^2}$.

The UAV flight process involves coordinate systems and angles, and the coordinate systems are the ground coordinate system and airframe coordinate system, respectively. The angles are the pitch angle of the UAV moving up and down, the yaw angle between the actual UAV heading and the planned heading, and the roll angle of the UAV moving left and right, respectively. In this paper, the UAV needs to maintain the uniform speed in the circular arc which involves the UAV steering problem, i.e., the roll angle of the UAV, as shown in Figure 5.

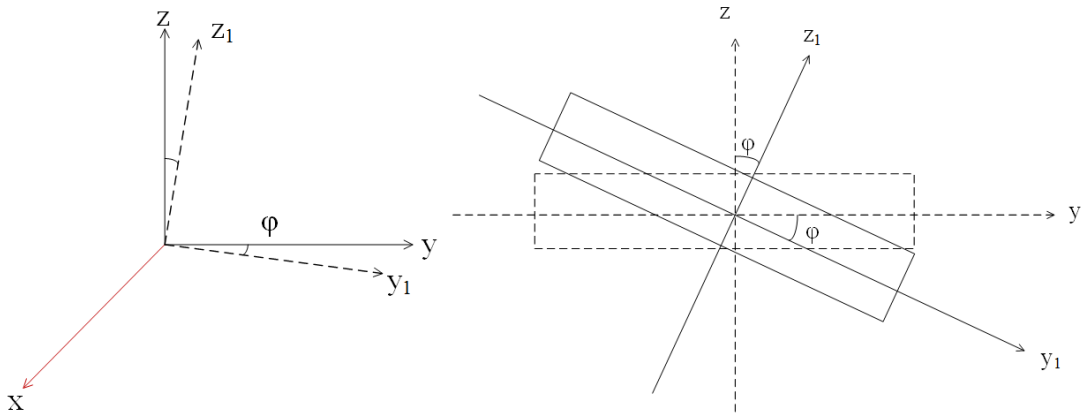

FIGURE 5. Diagram of rolling angle

Theorem 3.3. *It is supposed that the uniform speed through the arc is different because of the different roll angle φ of the UAV on the same circle, then the UAV needs to pass through the arc part with the maximum speed in the shortest time, and therefore, the maximum tumble angle $\varphi_{\max}$ of the UAV is needed. The force analysis of the UAV shows that when the maximum roll angle $\varphi_{\max}$ of the UAV is certain, the maximum speed v_{ci} through different obstacle circles O_i satisfies the following equation.*

$$v_{c_i} = \sqrt{gr_i \tan \varphi_{\max}} \tag{11}$$

The horizontal thrust and drag balance when the UAV is flying at a uniform speed in the circular arc, and then the following equation is satisfied.

$$P_{c_i} = k \left(gr_i \tan \varphi_{\max}\right)^{\frac{3}{2}} \tag{12}$$

where g is the acceleration of gravity. By Equations (11) and (12), it can be seen that the maximum speed v_{c_i} and acceleration power P_{c_i} of the UAV when passing through the arc of the obstacle circle are only related to the radius.

3.3. **Energy consumption model.** The battery of the UAV provides stable electrical energy for the system, which is amplified and controlled by ESC (electronic speed control) and transmitted to the motor, which converts the electrical energy into rotating mechanical energy and transmits it to the propeller, which generates tension and torque to provide lift and attitude control for the whole aircraft, as shown in Figure 6.

The optimal path generated by TPA consists of the straight line and part of the circular arc. The UAV flight path consists of multi-segment displacement, and each segment displacement process needs to determine the optimal acceleration and deceleration power and flight time for each segment displacement according to the actual flight of the UAV. Then the UAV energy consumption mode satisfies the following equation.

$$E_{res} = E_{sum} - \sum_{i=1}^{n} \left[\left(\frac{P_i}{\eta_{sum}} + P_{cecp} \right) \Delta t_i \right] \tag{13}$$

where E_{res} is the remaining battery energy of the UAV after the flight, E_{sum} is the total battery energy of the UAV before the mission, P_i is the moving power of the UAV flight, η_{sum} is the efficiency of the propeller to utilize the electrical energy from the battery, P_{cecp} is the fixed energy power of the UAV, and Δt_i is the time of each displacement of the UAV.

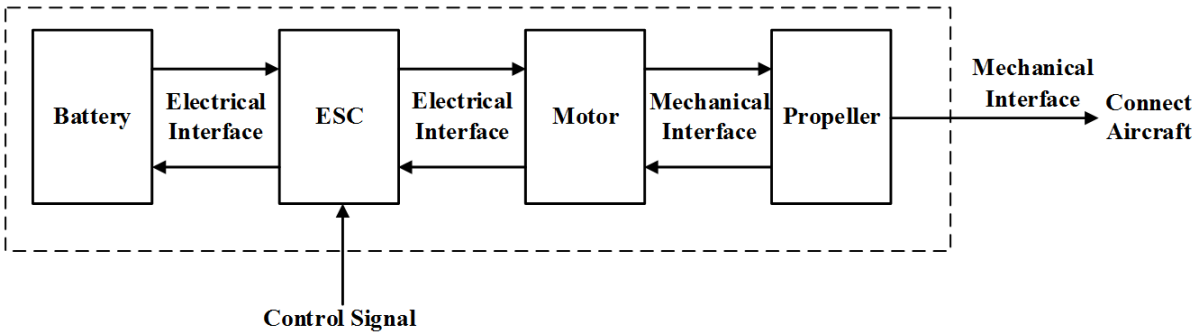

FIGURE 6. Flow chart of UAV energy transmission

The electrical power of the UAV flight is P_{ele}, the efficiency of the ESC using the electrical energy of the battery is η_1, the efficiency of the motor using the electrical energy of the ESC is η_2, the efficiency of the propeller using the mechanical energy of the motor is η_3, and then $P_{ele} = \frac{P_i}{\eta_{sum}} = \frac{P_i}{\eta_1\eta_2\eta_3}$. Fixed energy power P_{cecp} of the UAV includes but is not limited to the UAV hovering energy loss, on-board computing energy loss, sensor energy loss, data transmission energy loss, and other energy loss due to necessary operations. In particular, the UAV needs to calculate the energy consumption before performing the mission to ensure that the UAV has enough battery energy left to complete the mission to return to the flight, and the return path is the same as the path of the mission, i.e., the original path.

4. Algorithms and Strategies.

4.1. Optimal path algorithm – TPA.

The traditional graph-based path planning method mainly has two steps. The first step is to build a suitable map, and the second step is to find a high-quality collision-free path based on the starting and ending points on this map. It is usually necessary to generate many candidate paths to generate high-quality collision-free paths in the second step. However, if the scale of the map is relatively large and complex, it will not only increase the storage but also significantly reduce the computing efficiency because of the more candidate paths. Different from the traditional visualization-based path planning method, TPA does not traverse all common tangents between all obstacle circles. It finds the obstacle circles near the connection line between the starting point and ending point through the preliminary screening. The obstacle circles passing through the shortest path again are filtered out by some special rules, and then the common tangents are arranged between these obstacles and arcs in these obstacles. Finally, the shortest path is found by comparing the length of the paths.

Firstly, TPA needs to store the information of the starting and ending points and all obstacle circles on the map. The information includes the coordinates of the center of the circle and the radius. Then, the obstacle circles passing through the line connecting the starting and ending points are filtered, and these circles are recorded that the shortest path may pass through. It is also necessary to sort according to the distance between the center of the obstacle circle and the starting point since the position of the circle is disordered.

The shortest path does not necessarily pass through all the circles obtained in the initial screening, so further screening is required. It should be filtered from the starting point based on the distance from the ending point to the farthest obstacle, which can directly reach the ending point, and all other circles are removed between the two circles from the path. Then, the newly found circle is used as the starting point to find the farthest circle it can reach, and the cycle is repeated until the ending point is found. It is worth noting that even a circle closest to the starting point may not be directly reachable. In this case, it is necessary to find the tangent that passes through the circles at least among the four common tangents. Add these circles that this tangent passes through to the circles that the shortest path might go through and reorder.

After completing the above steps, all the circles passed by the shortest path can be obtained. Since these circles are sorted by distance, the shortest paths also pass through the circles in order. That is, the total path can be divided into segments, each of which is the common tangent to an adjacent circle and the corresponding arc. These common tangents are arranged and combined, and the tangent points corresponding to the common tangent points are combined to determine the arc on the same circle, and all paths from the starting point to the ending point can be obtained. This shortest path is the optimal path by comparing the lengths of all paths.

There is an example to understand the whole process of the TPA more clearly, as shown in Figure 7. Firstly, all the information of each obstacle circle including the starting point S and ending points E is stored in the figure. By judging the positional relationship between all circles and the line segment SE in the figure, the obstacle circles P_0, P_1, and P_2 can be classified as circles that the shortest path may pass through. After the first screening, the S is taken as the starting point to determine whether the common tangents of S-E, S-P_2, S-P_1, and S-P_0 have directly reached tangents. S-E and S-P_2 have successively judged that no tangent can be directly reached, while S-P_1 has tangents SA_1 and SA_2 that can be directly reached by the common tangent. The starting point S can directly reach the circle P_1. The P_0 is deleted from the circles that might be passed, only the circles P_1 and P_2 are left, and then use the circle P_1 as the starting point to judge whether the common tangents of P_1-E and P_1-P_2 have direct reaching tangents. P_1-E

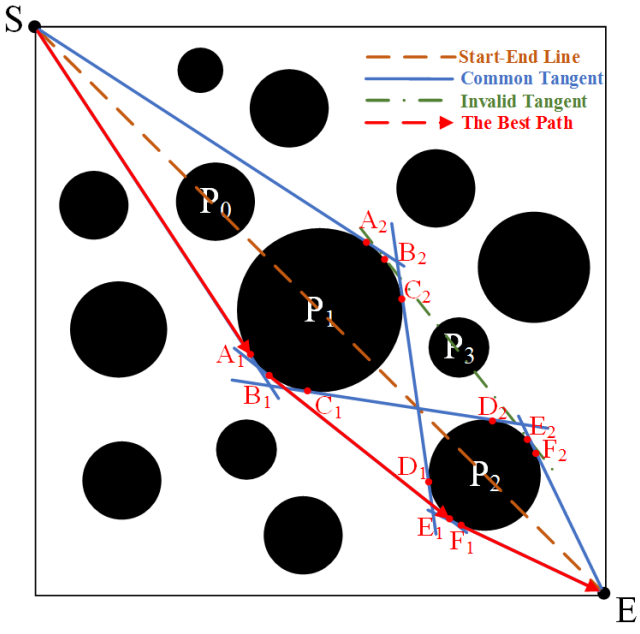

FIGURE 7. An example of the TPA generating a path in a known environment

has no tangent that can reach directly, while P_1-P_2 has tangents B_1E_1, C_1D_2, and C_2D_1 that the common tangent can reach directly, that is, the circle P_1 can directly reach the circle P_2. Finally, the circle P_2 is taken as the starting point to determine whether the common tangent of P_2-E has a direct tangent. P_2-E has tangents F_1E and F_2E that the common tangent can reach directly, that is, the circle P_2 can directly reach the ending point E, and the order of the circles passed by the shortest path is S-P_1-P_2-E.

The circle passed by the shortest path divides the shortest path into three segments named S-P_1, P_1-P_2, and P_2-E, respectively. S-P_1 segment has two sub-paths SA_1, SA_2, P_1-P_2 segment has three sub-paths B_1E_1, C_1D_2, C_2D_1 (the sub-path B_2E_2 is deleted because the tangent B_2E_2 passes through circle P_3), P_2-E segment has two sub-paths F_1E, F_2E, and after permutation and combination, there are 12 total paths. The length of the sub-path between different obstacle circles and the arc length on the same obstacle circle can be determined through the tangent points of each tangent. A path with the shortest total path length is selected as the optimal path, named SA_1-B_1E_1-F_1E.

The pseudocode of the TPA is shown in Figure 8 and the main procedure of the TPA is as follows.

Step 0 (Obstacle circle modeling): Randomly generate obstacle circles on the specified map, denoted as P_i, as shown in Figure 7.

Step 1 (Initialization): Add the information of all obstacle circles to the array Ob. The array TP is initialized as an empty array to store the tangent points information of obstacle circles that the shortest path may path through.

Step 2 (Preliminary screening): Add the circles that intersect the line between the starting and ending points to the array PC and reorder them and arrange them from the smallest to the largest according to the distance from the start point.

Step 3: Take the starting point as the first circle and the ending point as the second circle.

Step 4 (Make the common tangent): Make the common tangent of the two circles. It is worth noting that when the slope k of the common tangent tends to infinity, or the radiuses of the two circles are the same, the results of calculating the values of k and b respectively are not credible. Therefore, for the case where the common tangent is vertical, the square difference formula method can be used to simplify; when the radiuses of the two circles are equal, use the plane geometric translation trigonometric function method to find the relationship between the b value and the radius of the center coordinate.

Step 5 (Second screening): If two circles have at least one common tangent that does not pass through other circles, delete all circles between these circles in the array PC. Determine whether the second circle is the ending point: if so, skip to Step 7; otherwise, use the second circle as the first circle and skip to Step 4.

Step 6: If all the common tangents of the two circles pass through other circles, determine whether the two circles are adjacent.

Step 7 (Adding path tangent points): The two adjacent circles in the array PC make common tangents in turn, and add the tangent point information of the non-collision tangent points to the array TP in order, then add the number of tangents to the corresponding array Nm in the corresponding location. Common tangents between different circles are stored separately in the form of three-dimensional arrays to ensure logical calling.

Step 8 (Path encoding): The number of common tangents between the circles can be obtained from the set RN, so the number of total paths is the product of the number of common tangents. Divide each element of the array RN from 0 to n, and add a series of numbers to the set Nm row by row, which is the code of each total path. Divide 0$\sim$24 and $\{2, 4, 3\}$ in turn to get $\{0, 0, 0\}\sim\{1, 3, 2\}$, which are added to the array Nm in turn. After the encoding is completed, the tangent information can be called using the encoding and

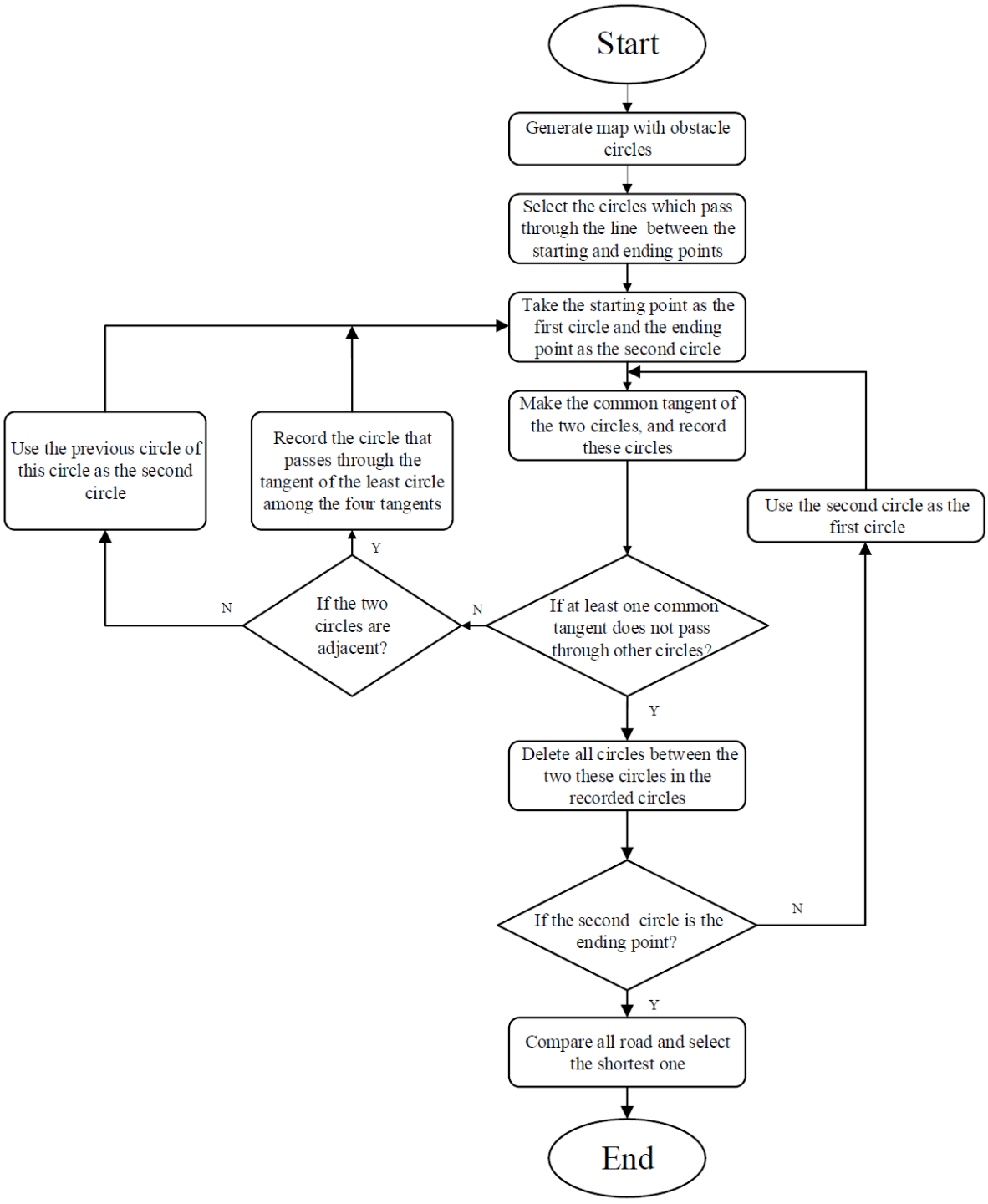

FIGURE 8. The pseudocode of the TPA

the array TP. The second index of the array TP is the size of the element in the array Nm, and the first index of the array TP is the column where the element is located. In this way, the required tangent information can be effectively searched.

Step 9 (Output the optimal path): Combining the tangent information in the set TP with the encoding of the set Nm, the shortest path is selected as the optimal path by calculating, and the tangent information of the optimal path is added to the Collection BR to output and end the program.

4.2. **Flight strategy.** The TPA algorithm can generate a satisfactory path. The UAV needs to determine the flight strategy on the shortest path to ensure the shortest time for the UAV to perform the mission after determining the flight path. According to the kinematics of the UAV, the physical model is determined. The UAV is accelerated and decelerated with constant power, and the air resistance is considered to ensure that the flight strategy is practical. At the same time, according to the number and information of obstacles between the starting and ending points, different flight modes of the UAV are determined, and the optimal flight mode of the UAV is selected according to the distance between obstacles, which lays a foundation for the optimal path combined with the optimal flight mode to determine the optimal flight strategy in the simulation stage.

1) **Start-End line without obstacles**

There is no obstacle on the start-end line of the mission performed by the UAV, and then the UAV flies directly from the starting point to the ending point along the line of the two points. It is assumed that the length of the straight line between the starting point and the ending point is l_{SE}, the maximum speed that the UAV can achieve is $v_{\max}$, the constant acceleration power of the UAV is P_{su}, the constant deceleration power is P_{sd}, and the air resistance of the UAV during flight is $f = kv^2$, as shown in Figure 9.

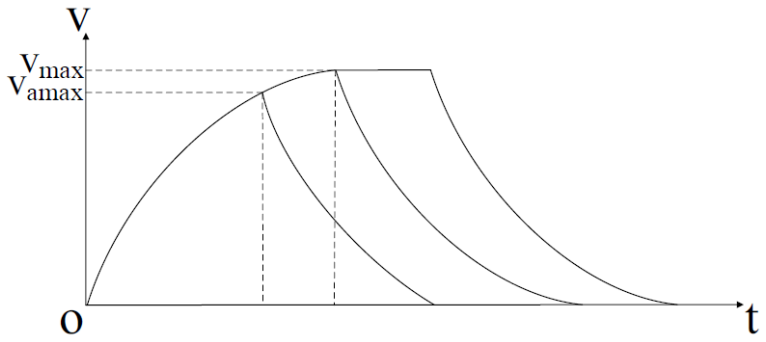

FIGURE 9. v-t diagram of the three flight modes without obstacles on the S-E line of the UAV

There are three flight modes of the UAV in the 0-0 straight-line segment. (a) The UAV's power changes abruptly from 0 to P_{su} at the point S and the UAV accelerates to $v_{\max}$ with maximum acceleration power P_{su} and then decelerates to 0 with maximum deceleration power P_{sd} to reach the point E at a distance of S_1. The power changes abruptly from P_{sd} to 0 at the point E. (b) When $0 < l_{SE} < S_1$, the UAV at the point S accelerates to $v_{a\max}$ with maximum acceleration power P_{su} and then decelerates to 0 with maximum deceleration power P_{sd} to reach the point E. (c) When $l_{SE} > S_1$, the UAV at the point S accelerates to $v_{\max}$ with maximum acceleration power P_{su}, flies evenly with maximum speed $v_{\max}$ for time t_{ep} and then decelerates to 0 with maximum deceleration power P_{sd} to reach the point E, where $t_{ep} = \frac{S_{ep}}{v_{\max}} = \frac{l_{SE}-S_1}{v_{\max}}$. According to Equations (6) and (8), the actual maximum speed $v_{a\max}$ is obtained to satisfy the following equation.

$$l_{SE} = S_{asu} + S_{asd} = \frac{m}{3k} \ln \left[\frac{P_{su}}{P_{sd}} \left(1 + \frac{P_{su} + P_{sd}}{P_{su} - kv_{a\max}^3} \right) \right] \tag{14}$$

2) **Start-End line with two or more obstacles**

There are two obstacles on the start-end line of the mission performed by the UAV, as shown in Figure 10. It is assumed that the acceleration power of the UAV passing in the arc of the first obstacle circle P_1 is P_{c_1} and the uniform velocity is v_{c_1}. The acceleration power of the UAV passing in the arc of the last obstacle circle P_2 is P_{c_2} and the uniform velocity is v_{c_2}. Only the minimum time is considered in the flight strategy in this process.

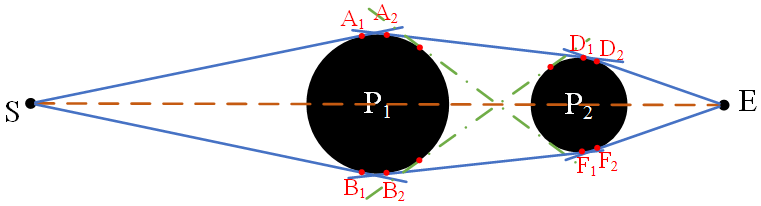

FIGURE 10. Two obstacles between the start-end line of the UAV

1) In terms of the arc of the UAV on the same obstacle circle, taking $\overset{\frown}{A_1A_2}$ as an example, the speed of the UAV at the point A_1 is v_{c_1}, and the power is acceleration power P_{c_1}. At this time, thrust and resistance of the UAV are the same, the UAV starts to do a uniform speed circular motion to the point A_2 with the maximum rolling angle $\varphi_{\max}$, the speed size of the UAV at the point A_2 is still v_{c_1}, and the power is still acceleration power P_{c_1}. Among them, the UAV flight time is $t_{c_1} = \frac{\overset{\frown}{A_1A_2}}{v_{c_1}}$.

2) All the flight modes of the UAV in the acceleration straight section between the starting point and the obstacle and the deceleration straight section between the obstacle and the ending point are shown in Figure 11. There are five ways in the 0-v_{c_1} acceleration straight section of the UAV, the power is P_{c_1} and the speed is v_{c_1} at the first obstacle circle regardless of the flight mode. l_{SA_1} is taken as an example, the UAV's power changes abruptly from 0 to P_{su} at the point S and it accelerates to v_{c_1} with maximum acceleration power P_{su} to reach the point A_1 at a distance of S_0, the power changes abruptly from P_{su} to P_{c_1} at the point A_1; the UAV at the point S accelerates to $v_{\max}$ with maximum acceleration power P_{su} and decelerates to v_{c_1} with maximum deceleration power P_{sd} to reach the point A_1 at a distance of S_1, the power changes abruptly from P_{sd} to P_{c_1} at the point A_1; when $S_0 < l_{SA_1} < S_1$, the UAV at the point S accelerates to $v_{a\max}$ with maximum acceleration power P_{su} and decelerates to v_{c_1} with maximum deceleration power P_{sd} to reach the point A_1; when $l_{SA_1} > S_1$, the UAV at the point S accelerates to $v_{\max}$ with maximum acceleration power P_{su}, flies evenly with maximum speed $v_{\max}$ for time t_{ep} and then decelerates to v_{c_1} with maximum deceleration power P_{sd} to reach the point A_1, where $t_{ep} = \frac{S_{ep}}{v_{\max}} = \frac{l_{SA_1}-S_1}{v_{\max}}$; specifically, $P_{su} = P_{c_1}$ when $v_{c_1} = v_{\max}$, the UAV at the point S accelerates to $v_{\max}$ with maximum acceleration power P_{su}, flies evenly with maximum speed $v_{\max}$ for time t_{ep} to reach the point A_1, where the power is constant at the point A_1 and $t_{ep} = \frac{S_{ep}}{v_{\max}} = \frac{l_{SA_1}-S_1}{v_{\max}}$. The length l_{SA_1} of the acceleration straight section of the UAV between the starting point and the obstacle is constrained to $l_{SA_1} \geq S_0$.

There are five ways in the v_{c_2}-0 deceleration straight section of the UAV, the power is P_{c_2} and the speed is v_{c_2} at the last obstacle circle regardless of the flight mode. l_{D_2E} is

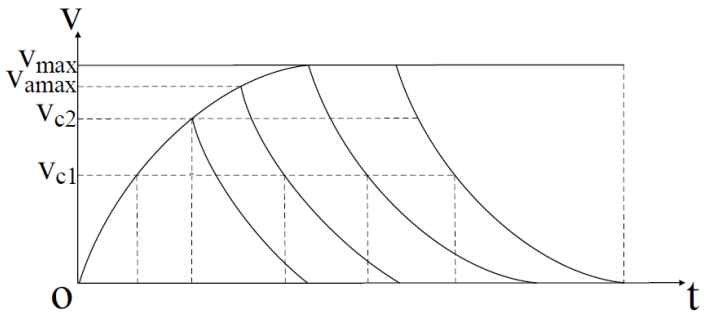

FIGURE 11. v-t diagram of the flight modes of the UAV between the start-end points and the obstacle, respectively

taken as an example, the UAV's power changes abruptly from P_{c_2} to P_{sd} at the point D_2 and it decelerates from v_{c_2} to 0 with maximum deceleration power P_{sd} to reach the point E at a distance of S_0, the power changes abruptly from P_{sd} to 0 at the point E; the UAV's power changes abruptly from P_{c_2} to P_{su} at the point D_2, then the UAV accelerates to $v_{\max}$ with maximum acceleration power P_{su} and decelerates to 0 with maximum deceleration power P_{sd} to reach the point E at a distance of S_1; when $S_0 < l_{D_2E} < S_1$, the UAV at the point D_2 accelerates to $v_{a\max}$ with maximum acceleration power P_{su} and decelerates to 0 with maximum deceleration power P_{sd} to reach the point E; when $l_{D_2E} > S_1$, the UAV at the point D_2 accelerates to $v_{\max}$ with maximum acceleration power P_{su}, flies evenly with maximum speed $v_{\max}$ for time t_{ep} and then decelerates to 0 with maximum deceleration power P_{sd} to reach the point E, where $t_{ep} = \frac{S_{ep}}{v_{\max}} = \frac{l_{D_2E}-S_1}{v_{\max}}$; specifically, $P_{su} = P_{c_2}$ when $v_{c_2} = v_{\max}$, the UAV at the point D_2 flies evenly with maximum speed $v_{\max}$ for time t_{ep} and then decelerates to 0 with maximum deceleration power P_{sd} to reach the point E, where the power is constant at the point D_2 and $t_{ep} = \frac{S_{ep}}{v_{\max}} = \frac{l_{D_2E}-S_0}{v_{\max}}$. The length l_{D_2E} of the deceleration straight section of the UAV between the obstacle and the ending point is constrained to $l_{D_2E} \geq S_0$.

3) All flight patterns of the drone in the acceleration straight section, deceleration straight section and straight section between two obstacles are shown in Figure 12. When $v_{c_1} < v_{c_2}$, there are five ways in the v_{c_1}-v_{c_2} acceleration straight section of the UAV, regardless of the flight mode, the power is P_{c_1} and the speed is v_{c_1} at the first obstacle circle; the power is P_{c_2} and the speed is v_{c_2} at the second obstacle circle. $l_{A_2D_1}$ is taken as an example, the UAV's power changes abruptly from P_{c_1} to P_{su} at the point A_2 and the UAV accelerates to v_{c_2} with maximum acceleration power P_{su} to reach the point D_1 at a distance of S_0, the power changes abruptly from P_{su} to P_{c_2} at the point D_1; the UAV at the point A_2 accelerates from v_{c_1} to $v_{\max}$ with maximum acceleration power P_{su} and decelerates to v_{c_2} with maximum deceleration power P_{sd} to reach the point D_1 at a distance of S_1, the power changes abruptly from P_{sd} to P_{c_2} at the point A_1; when $S_0 < l_{A_2D_1} < S_1$, the UAV at the point A_2 accelerates from v_{c_1} to $v_{a\max}$ with maximum acceleration power P_{su} and decelerates to v_{c_2} with maximum deceleration power P_{sd} to reach the point D_1; when $l_{A_2D_1} > S_1$, the UAV at the point A_2 accelerates from v_{c_1} to $v_{\max}$ with maximum acceleration power P_{su}, flies evenly with maximum speed $v_{\max}$ for time t_{ep} and then decelerates to v_{c_2} with maximum deceleration power P_{sd} to reach the point D_1, where $t_{ep} = \frac{S_{ep}}{v_{\max}} = \frac{l_{A_2D_1}-S_1}{v_{\max}}$; specifically, $P_{su} = P_{c_2}$ when $v_{c_2} = v_{\max}$, the UAV at the point A_2 accelerates to $v_{\max}$ with maximum acceleration power P_{su}, flies evenly with maximum speed $v_{\max}$ for time t_{ep} to reach the point D_1, where the power is constant at the point D_1 and $t_{ep} = \frac{S_{ep}}{v_{\max}} = \frac{l_{A_2D_1}-S_0}{v_{\max}}$. The length $l_{A_2D_1}$ of the acceleration straight section of the UAV between two obstacles is constrained to $l_{A_2D_1} \geq S_0$.

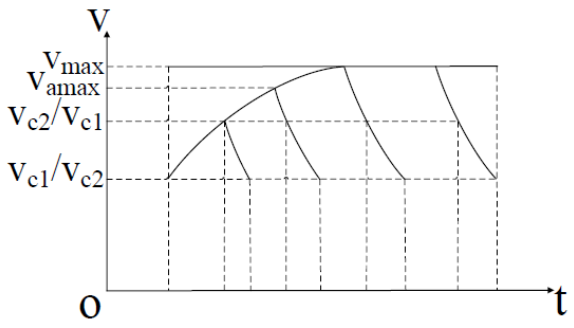

FIGURE 12. v-t diagram of the flight modes between two obstacles of the UAV

When $v_{c_1} > v_{c_2}$, there are five ways in the v_{c_1}-v_{c_2} deceleration straight section of the UAV, regardless of the flight mode, the power is P_{c_1} and the speed is v_{c_1} at the first obstacle circle; the power is P_{c_2} and the speed is v_{c_2} at the second obstacle circle. $l_{A_2D_1}$ is taken as an example, the UAV's power changes abruptly from P_{c_1} to P_{sd} at the point A_2 and it decelerates to v_{c_2} with maximum deceleration power P_{sd} to reach the point D_1 at a distance of S_0, the power changes abruptly from P_{sd} to P_{c_2} at the point D_1; the UAV's power changes abruptly from P_{c_1} to P_{su} at the point A_2, then the UAV accelerates from v_{c_1} to $v_{\max}$ with maximum acceleration power P_{su} and decelerates to v_{c_2} with maximum deceleration power P_{sd} to reach the point D_1 at a distance of S_1; when $S_0 < l_{A_2D_1} < S_1$, the UAV at the point A_2 accelerates from v_{c_1} to $v_{a\max}$ with maximum acceleration power P_{su} and decelerates to v_{c_2} with maximum deceleration power P_{sd} to reach the point D_1; when $l_{A_2D_1} > S_1$, the UAV at the point A_2 accelerates from v_{c_1} to $v_{\max}$ with maximum acceleration power P_{su}, flies evenly with maximum speed $v_{\max}$ for time t_{ep} and then decelerates to v_{c_2} with maximum deceleration power P_{sd} to reach the point D_1, where $t_{ep} = \frac{S_{ep}}{v_{\max}} = \frac{l_{A_2D_1}-S_1}{v_{\max}}$; specifically, $P_{su} = P_{c_1}$ when $v_{c_1} = v_{\max}$, the UAV at the point A_2 flies evenly with maximum speed $v_{\max}$ for time t_{ep} and then decelerates to v_{c_2} with maximum deceleration power P_{sd} to reach the point D_1, where the power is constant at the point A_2 and $t_{ep} = \frac{S_{ep}}{v_{\max}} = \frac{l_{A_2D_1}-S_0}{v_{\max}}$. The length $l_{A_2D_1}$ of the deceleration straight section of the UAV between two obstacles is constrained to $l_{A_2D_1} \geq S_0$.

When $v_{c_1} = v_{c_2}$, there are four ways in the v_{c_1}-v_{c_2} straight section of the UAV, regardless of the flight mode, the power is P_{c_1} and the speed is v_{c_1} at the first obstacle circle; the power is P_{c_2} and the speed is v_{c_2} at the second obstacle circle. $l_{A_2D_1}$ is taken as an example, the UAV's power changes abruptly from P_{c_1} to P_{su} at the point A_2, then the UAV accelerates from v_{c_1} to $v_{\max}$ with maximum acceleration power and decelerates to v_{c_2} with maximum deceleration power P_{sd} to reach the point D_1 at a distance of S_1, the power changes abruptly from P_{su} to P_{c_2} at the point D_1; when $0 < l_{A_2D_1} < S_1$, the UAV at the point A_2 accelerates from v_{c_1} to $v_{a\max}$ with maximum acceleration power P_{su} and decelerates to v_{c_2} with maximum deceleration power P_{sd} to reach the point D_1; when $l_{A_2D_1} > S_1$, the UAV at the point A_2 accelerates from v_{c_1} to $v_{\max}$ with maximum acceleration power P_{su}, flies evenly with maximum speed $v_{\max}$ for time t_{ep} and then decelerates to v_{c_2} with maximum deceleration power P_{sd} to reach the point D_1, where $t_{ep} = \frac{S_{ep}}{v_{\max}} = \frac{l_{A_2D_1}-S_1}{v_{\max}}$; specifically, $P_{su} = P_{c_1} = P_{c_2}$ when $v_{c_1} = v_{c_2} = v_{\max}$, the UAV at the point A_2 flies evenly with maximum speed $v_{\max}$ for time t_{ep} and then decelerates to v_{c_2} with maximum deceleration power P_{sd} to reach the point D_1, where the power is constant at the point A_2 and $t_{ep} = \frac{l_{A_2D_1}}{v_{\max}}$.

In summary, the two adjacent obstacle circles (including the start-end points) on the optimal path of the UAV are successively represented by P_i and P_{i+1}. Then the flight strategy is divided into three categories, of which the three common modes of motion are as follows: the UAV accelerates from v_i to $v_{a\max}$ and then decelerates to v_{i+1}; the UAV accelerates from v_i to $v_{\max}$ and then decelerates to v_{i+1}; the UAV accelerates from v_i to $v_{\max}$ and maintains $v_{\max}$ for times and then decelerates to v_{i+1}. In particular, in the first category, when $0 \leq v_i < v_{i+1}$, there are such two modes that the UAV accelerates from v_i to v_{i+1}, and accelerates from v_i to v_{i+1} and starts at a constant speed. In the second category, when $v_i = v_{i+1} \neq 0$, there is the mode that the UAV makes uniform motion from v_i to v_{i+1}. In the third category, when $v_i > v_{i+1} \geq 0$, there are such two modes that the UAV decelerates from v_i to v_{i+1}, and the UAV makes uniform motion by v_i and decelerates to v_{i+1}.

5. **Simulation Results.** The TPA and three comparison algorithms A*, PRM and RRT proposed in this paper are simulated in the map with different environmental complexity, and the path length and computational time of the four algorithms are compared to prove the superiority of TPA by calling the cv2 packet in Python. At the same time, the UAV motion process is encoded and simulated in MATLAB, and the bi-objective optimal solution is obtained, which is combined with the optimal path of TPA to obtain the optimal flight strategy of each sub-path. The above algorithm program runs on the PC with a core i7-10750H 2.60GHz CPU, 16G memory, and the Windows operating system.

The time complexity of the TPA is extremely low, and the path generated is relatively smooth. Thus, high-performance MCU and high-power motors are not required, and micro-UAVs can meet the hardware conditions required for TPA. Therefore, when simulating the motion process, the technical parameters which refer to the DJI Air 2S UAV are adjusted to simplify the calculation process. The parameters and values of the computer simulation of the UAV motion process are shown in Table 2. Among them, the UAV drag coefficient is $k = \frac{1}{2}C\rho A = 0.0125$.

Table 2. Parameters used in simulations

Parameter	Meaning	Value
C	Coefficient of air drag	0.1
ρ	Air density	1.29 kg/m^3
A	Blocked area of UAV	0.1938 m^2
m	UAV mass	1 kg
$v_{\max}$	Maximum horizontal linear speed	0-20 m/s
P_{su}	UAV acceleration power	0-100 w
P_{sd}	UAV deceleration power	0-100 w
$\varphi_{\max}$	The maximum roll angle of a UAV	30°

5.1. **Optimal path simulation.** Considering the practical application and scene of the UAV, the maximum speed of the UAV does not exceed 20 m/s. According to Equation (11), it can be known that the radius of the obstacle circle does not exceed 70 m. This article stipulates that the radiuses of the randomly generated obstacle circle are 15 m-40 m, and the map is determined to be a square area of 500 m * 500 m. The starting point of the UAV is taken as the origin, the horizontal right is the x-axis, and the horizontal downward is the y-axis to establish a plane rectangular coordinate system. The coordinate of the ending point of the drone is $(500, 500)$, and the straight-line distance between the starting and ending points is 707.11 m.

To obtain the comparison reliability of the path planning performance of TPA and the other three algorithms, the obstacle circles in the map of the simulation experiment should be considered in the different layout structures. Therefore, as shown in Figure 13, a total of six types of environments in two categories have been designed, each has unique spatial characteristics, and the six environments are labeled E1-E6, where (a) E1, a simple environment with single obstacle circles; (b) E2, a simple environment for tangent obstacle circles; (c) E3, a simple environment for a combination of single and tangent obstacle circles; (d) E4, a complex environment with single obstacle circles; (e) E5, complex environment of tangent obstacle circles; (f) E6, complex environment with a combination of single and tangent obstacle circles. Simple environments E1-E3 are environments with 10 individual obstacle circles, 5 pairs of tangent obstacle circles, 4 individual obstacle circles, and 4 pairs of tangent obstacle circles combined. The complex environments E4-E6 are environments with 30 individual obstacle circles, 15 pairs of

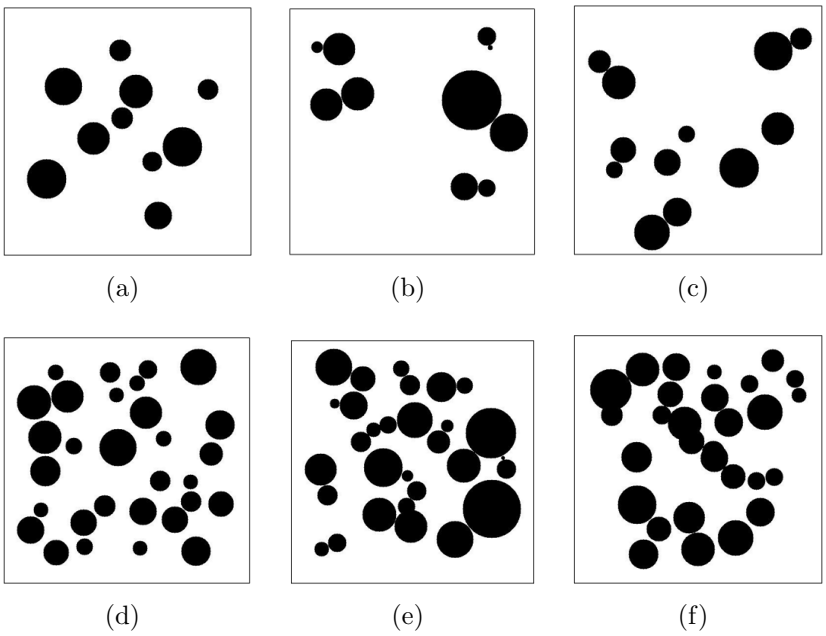

FIGURE 13. Six different environments E1-E6

tangent obstacle circles, 14 individual obstacle circles and 8 pairs of tangent obstacle circles, respectively. There are two reasons for designing the environment of the tangent obstacle circle: 1) The distance between buildings is very short in the real environment, and the intersection of obstacle circles need not be considered because the building group can be directly reconstructed into obstacle circles with a larger radius; 2) When the number of intersecting obstacle circles is large, it is easy to simulate a simple trap-like environment, which proves the ability of the TPA to escape traps.

This section compares the path length and computing time generated by the TPA, A*, PRM, and RRT under six instances of different environments E1-E6, which are shown in Table 3 and Figure 14. The four algorithms can control the single variable by the type of environment or the number and type of obstacles, and compare the path length and computational time of the experimental results horizontally and vertically. It can be seen from the data in Table 3 that, in the instance under the same environment, compared with the other three algorithms, the path length and computing time of the paths generated by the TPA are the shortest. The A* algorithm has the longest computational time, but its path length is just better than RRT. The RRT has the longest path length, but its computational time is second only to TPA. The PRM has a relatively balanced path length and computational time, but the quality is not as good as TPA. Compared with

TABLE 3. Experimental results of the four algorithms in six different environments

Env	Type	Path length (m)				Computing time (sec)			
		TPA	A*	PRM	RRT	TPA	A*	PRM	RRT
E1	10+0	714.00	736.40	711.53	849.70	0.078	1.286	0.891	0.532
E2	0+5*2	736.00	768.11	748.65	895.78	0.078	1.343	0.938	0.485
E3	4+4*2	717.00	772.25	807.81	753.19	0.078	1.312	0.844	0.562
E4	16+0	729.00	791.54	753.61	871.09	0.109	1.094	0.562	0.594
E5	0+8*2	746.00	784.79	775.43	871.52	0.094	1.560	0.641	0.500
E6	8+4*2	716.00	819.76	787.33	801.98	0.109	1.250	0.578	0.516

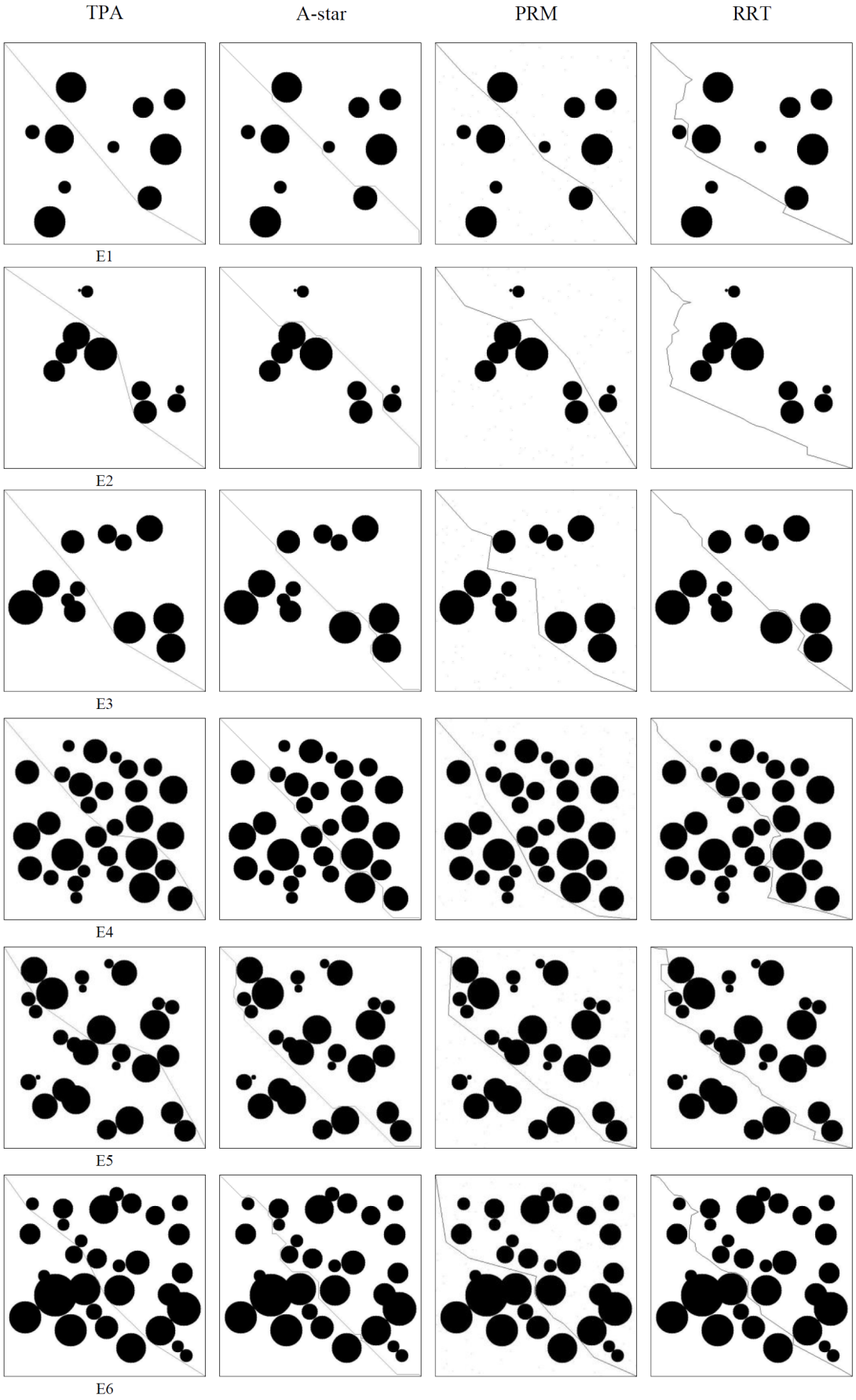

FIGURE 14. Paths generated by four algorithms in six different environments

the simple environment, in the complex environment example, the path length of the TPA does not fluctuate much, while the path length of the other three algorithms shows a large upward trend as a whole. The computational time of the algorithm shows a small upward trend, but the computational time of TPA is still much smaller than the other three algorithms. The path length and computing time of the TPA in the simple environment E1-E3 and the complex environment E4-E6 instances respectively have little fluctuation, while the other three algorithms fluctuate greatly.

Table 4. Experimental results of the four algorithms for 36 instances in six different environments

Instance	Env	Type	Path length (m)				Computing time (sec)			
			TPA	A*	PRM	RRT	TPA	A*	PRM	RRT
N1	E1	10+0	719.00	758.11	748.10	751.45	0.078	1.438	0.922	0.469
N2	E1	10+0	706.00	744.68	716.50	739.18	0.094	1.453	0.890	0.437
N3	E1	12+0	710.00	750.54	736.22	738.67	0.094	1.281	0.875	0.469
N4	E1	12+0	735.00	763.97	732.88	738.02	0.109	1.250	0.797	0.500
N5	E1	14+0	718.00	779.83	763.77	759.18	0.094	1.328	0.828	0.500
N6	E1	14+0	708.00	768.11	757.43	776.45	0.094	1.468	0.814	0.687
N7	E2	0+5*2	713.00	766.40	752.46	773.82	0.094	1.495	0.907	0.453
N8	E2	0+5*2	719.00	812.51	759.18	783.37	0.094	2.265	0.855	0.469
N9	E2	0+6*2	709.00	730.54	713.79	728.65	0.094	1.373	0.890	0.453
N10	E2	0+6*2	714.00	885.94	794.21	843.90	0.094	2.891	0.814	0.531
N11	E2	0+7*2	710.00	746.40	719.85	747.12	0.094	1.273	0.905	0.500
N12	E2	0+7*2	728.00	820.47	774.87	828.98	0.094	1.844	0.828	0.547
N13	E3	4+3*2	706.00	724.68	714.81	714.31	0.094	1.265	0.859	0.453
N14	E3	4+3*2	709.00	805.18	752.87	773.56	0.078	1.750	0.781	0.532
N15	E3	6+3*2	720.00	742.25	711.74	775.49	0.078	1.265	0.875	0.672
N16	E3	6+3*2	709.00	817.40	764.68	776.05	0.094	1.343	0.859	0.453
N17	E3	6+4*2	711.00	746.40	751.53	757.65	0.078	1.328	0.765	0.500
N18	E3	6+4*2	708.00	756.40	720.59	736.41	0.078	1.290	0.829	0.500
N19	E4	26+0	715.00	781.86	758.07	775.38	0.094	1.297	0.719	0.484
N20	E4	26+0	735.00	781.54	760.34	779.74	0.203	1.172	0.666	0.594
N21	E4	28+0	754.00	793.26	777.98	797.48	0.094	1.203	0.656	0.547
N22	E4	28+0	735.00	736.40	748.94	768.83	0.078	1.109	0.641	0.515
N23	E4	30+0	713.00	777.40	745.00	793.21	0.094	1.187	0.656	0.594
N24	E4	30+0	755.00	787.40	774.46	825.45	0.109	1.093	0.640	0.672
N25	E5	0+13*2	724.00	774.79	745.10	769.72	0.094	1.187	0.766	0.517
N26	E5	0+13*2	710.00	762.25	728.34	748.98	0.094	1.359	0.765	0.485
N27	E5	0+14*2	718.00	833.97	783.75	852.09	0.094	1.703	0.719	0.547
N28	E5	0+14*2	729.00	758.11	727.77	757.56	0.078	1.187	0.719	0.479
N29	E5	0+15*2	729.00	856.69	753.26	859.02	0.094	1.390	0.719	0.547
N30	E5	0+15*2	737.00	809.12	790.05	868.16	0.094	1.281	0.703	0.605
N31	E6	12+7*2	719.00	773.58	787.56	768.65	0.094	1.156	0.609	0.490
N32	E6	12+7*2	746.00	797.40	759.83	846.16	0.094	1.141	0.672	0.685
N33	E6	14+7*2	749.00	794.47	765.28	814.00	0.094	1.187	0.641	0.526
N34	E6	14+7*2	733.00	802.76	777.50	785.77	0.094	1.343	0.714	0.512
N35	E6	14+8*2	711.00	729.65	708.13	738.34	0.078	1.219	0.656	0.500
N36	E6	14+8*2	724.00	835.30	779.32	846.24	0.094	1.375	0.734	0.527

To obtain reliable results about the performance of TPA planning paths, the experimental results of the four algorithms in multiple simulations in different environments are shown in Table 4, with a total of 36 instances. Instances N1-N6, N7-N12, N13-N18, N19-N24, N25-N30, and N31-N36 are simulated in different environments E1-E6, while the instances Ni-N$i+1$ ($i = 1, 3, 5, \ldots, 33, 35$) have the same number and type of obstacle circles, but the specific obstacle locations are different. As shown in Figure 15 and Figure 16, the path length and computational time of the four algorithms in different environments are compared and analyzed through the experimental results of 36 instances.

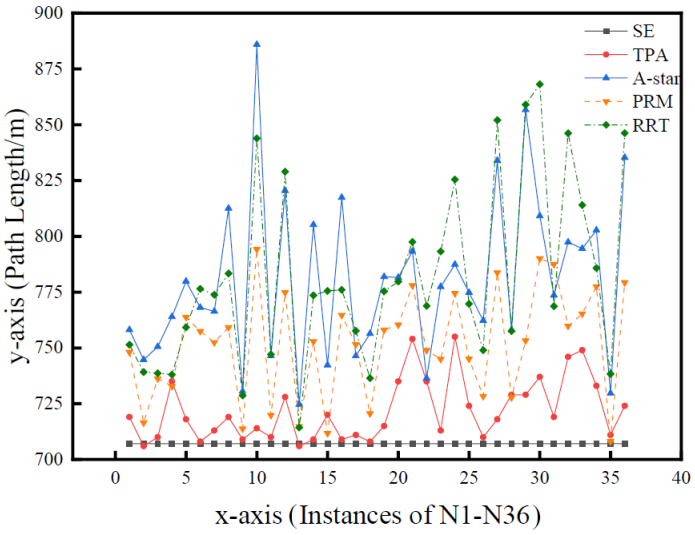

FIGURE 15. Comparison diagram of the path length of four algorithms in 36 examples

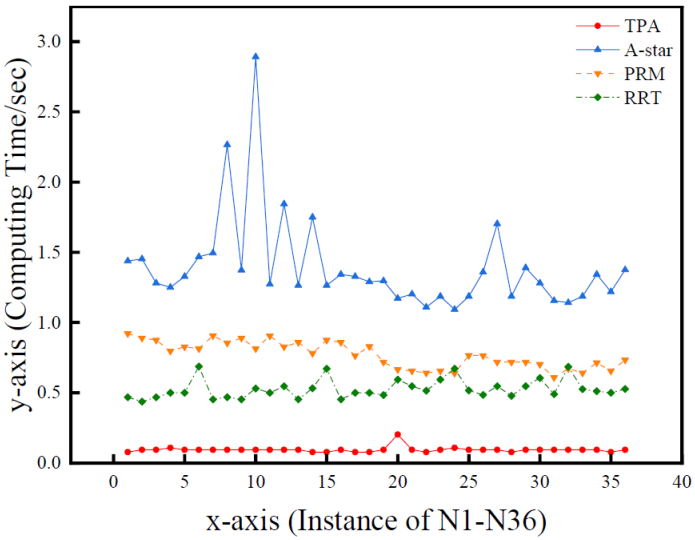

FIGURE 16. Comparison diagram of computing time of four algorithms in 36 examples

It can be seen from Figure 15 that the shortest path is generated through the TPA in each instance, and its path length is closest to the SE straight-line distance between the starting and ending points, which shows that the TPA has ability to generate the shortest path in both simple and complex environments. The TPA traverses the common tangent

between the starting point and the ending point and the adjacent obstacle circles. And the shortest path is selected by combining the sub-paths, comparing the total length. The grid-based deterministic algorithm A* can always assemble a path to the ending point in the vicinity of the obstacle circle, but the worst path is obtained in simple environmental instances. The classical RRT based on the characteristics of random sampling can ensure the generation of paths and has the ability to avoid simple traps. Nevertheless, the path length does not perform well in complex environment instances, and it is easy to generate some useless detour paths. In contrast, the PRM based on randomly scattered points performs well in all instances but still cannot guarantee the optimality of the path.

It can be seen from Figure 16, TPA can always generate the shortest collision-free path for each instance with the shortest computing time among the four algorithms. The A* has the longest computing time. The TPA has the shortest computational time, because it mainly generates the tangent points on each obstacle circle through the relevant computational formulas of the environment model and the motion model. And it finds the shortest path through the combination of sub-paths between the tangent points. Paths generated by TPA can avoid unnecessary detours. The RRT randomly samples from the starting point to the ending point, and the computational time of RRT is short. Oppositely, the PRM takes a long time to find the path by randomly picking points and connecting them in the obstacle-free area, so the A* algorithm takes the longest time to find the path by gridding the map. Table 4 also shows that the more obvious advantages of TPA in terms of computing time in the more complex environments.

All in all, compared with the other three algorithms, the TPA exhibits superior path planning performance in terms of path length and computing time in both simple and complex environments.

5.2. **Kinematic simulation and bi-objective optimization.** In the UAV kinematic model, the process of UAV performing the mission mainly consists of the acceleration flight process, the uniform speed flight process and the deceleration flight process. From Equations (11) and (12), it can be seen that the maximum speed v_{c_i} and acceleration power P_{c_i} of the UAV in uniform flight are fixed and only related to the radius r_i of the obstacle circle O_i, and then the flight time and energy consumption of the UAV flight process are related to the UAV acceleration and deceleration process. The flight strategy and optimal power are selected based on the information of the obstacle circle that the optimal path passes through to ensure the shorter UAV flight time and flight energy consumption.

1) Acceleration process

The UAV accelerates from 0 to the maximum speed $v_{\max}$ with a constant acceleration power P_{su} during the acceleration process, and the UAV acceleration time is $t_{\max}$. From Equation (7), it can be seen that the time t is related to the power P and speed v, that is, the power P determines the maximum speed v that the UAV can reach, while the power P and speed v determine the time t for the UAV to reach the maximum speed; thus, the different energy consumption can be produced. The greater the power, the smaller the time for the UAV to reach the maximum speed and the greater the energy consumption, which can be further clarified according to the functional equation simulation. Then, selecting the right power is a key step to ensure that the time to reach the maximum speed is short, the maximum speed meets the actual demand, and the energy consumption is low.

To investigate the relationship between the maximum speed, variables, time, energy consumption and power of the UAV, the acceleration power P was traversed from 1 to 100 w in steps of 1. The v-P, y-P, abs(y-1)-P, t-P, and w-P plots were simulated as shown in Figures 17(a)-17(e), where (a) v-P, maximum velocity versus power; (b) y-P,

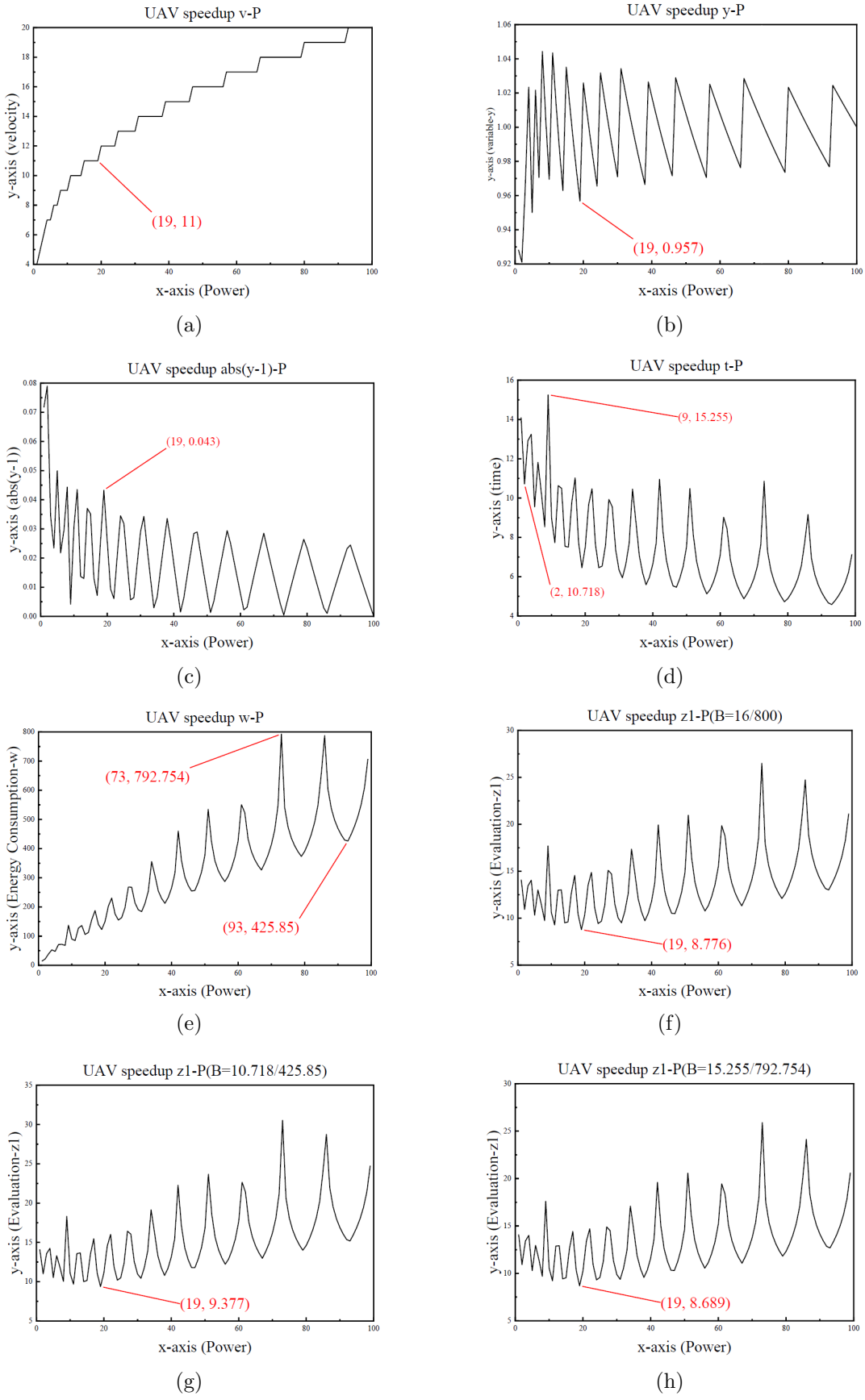

FIGURE 17. Relationship between motion parameters and bi-objective evaluation function versus power for the acceleration process of the UAV (a)-(h)

relationship between variable y and power; (c) abs(y-1)-P, the relationship between the variable abs(y-1) and power; (d) t-P, time of acceleration to maximum velocity versus power; (e) w-P, the energy consumption of the acceleration process versus power. In the v-P plot, the maximum speed of the UAV increases as the power increases; in the y-P plot, y-P is an oscillation curve with the variable y oscillating around 1, and the UAV reaches its maximum speed when y tends to 1; in the abs(y-1)-P plot, it is again verified that abs(y-1) oscillates around 0, resulting in an oscillation curve in the t-P plot, but the overall curve tends to fall; the w-P plot is also an oscillation curve because of $w = Pt$, but the overall curve tends to rise, following the law of motion.

When the weighting method is used to find the optimal solution for the bi-objective of UAV flight time and energy consumption, it is necessary to compare the bi-objective evaluation values of different weighting coefficients to determine the flight time weighting coefficient A and the flight energy consumption weighting coefficient B. Firstly, three sets of weighting coefficients are selected, as can be seen from the t-P and w-P images of the UAV acceleration process in Figures 17(d) and 17(e), the t-range is 16 and the w-range is 800, then the B coefficient is taken as 16/800 and the A factor is 784/800; the maximum value in the t minima is 10.718 and the maximum value in the w minima is 425.85, then the B factor is taken as 10.718/425.85 and the A factor is taken as 415.132/425.85; the maximum value of t is 15.255 and the maximum value of w is 792.754, then the B factor is taken as 15.255/792.754 and the A factor is taken as 777.499/792.754.

The simulation results are shown in Figures 17(f)-17(h), where (f) $z1$-P, the relationship between the bi-objective evaluation function of the first set of weighting coefficients and power; (g) $z1$-P, bi-objective evaluation function of the second set of weighting coefficients versus power; (h) $z1$-P, the bi-objective evaluation function of the third group of weighting coefficients versus power.

When the B coefficient is 16/800 and the A coefficient is 784/800, the bi-target evaluation $z1$ is 8.776; when the B coefficient is 10.718/425.85 and the A coefficient is 415.132/425.85, the bi-target evaluation $z1$ is 9.377; when the B coefficient is 15.255/792.754 and A coefficient is 777.499/792.754, the bi-target evaluation $z1$ is 8.689. By comparing the size of the bi-target evaluation $z1$, the weighting coefficient of the UAV acceleration process A coefficient is 777.499/792.754 and B coefficient is 15.25/792.754, and the optimal UAV acceleration power is 19 w. The v-P image shows that the speed is 11 m/s when the power is 19 w from Figure 17(a). Meanwhile, the optimal acceleration power of the UAV accelerated to different maximum speeds can be determined by combining Figures 17(a) and 17(h) as shown in Table 5.

Table 5. Optimal acceleration power for different maximum speeds of UAV

$v_{\max}$ (m/s)	≤ 11	12	13	14	15	16	17	18	19	20
P_{su} (w)	19	24	25	31	46	47	57	67	80	93

2) Deceleration process

The UAV decelerates from the maximum speed $v_{\max}$ to 0 with a constant deceleration power P_{sd} during the deceleration process, and the UAV deceleration time is $t_{\max}$. In order to facilitate the expression and calculation, the UAV deceleration physical model into the acceleration physical model, that is, the UAV accelerates from 0 to the maximum speed $v_{\max}$ with a constant acceleration power P_{su} during the acceleration process, and the movement time does not change. From Equation (9), it can be seen that the relationship between time t, power P and speed v is the same as the acceleration process, that is, the power P determines the maximum speed v that the UAV can reach, while the power P

and speed v determine the time t for the UAV to reach the maximum speed, resulting in different energy consumption.

To investigate the relationship between the maximum speed, variables, time, energy consumption and power of the UAV, the deceleration power P was traversed from 1 to 100 w in steps of 1. The v-P, x-P, (2-x)-P, t-P and w-P plots were simulated as shown in Figures 18(a)-18(e), where (a) v-P, maximum velocity versus power; (b) x-P, the relationship between variable x and power; (c) (2-x)-P, the relationship between the variable (2-x) and power; (d) t-P, the time of deceleration to maximum velocity versus power; (e) w-P, the energy consumption of the deceleration process versus power.

In the v-P plot, the maximum speed of the UAV increases as the power increases; in the x-P plot, x-P is an oscillation curve but the variables x are all below 2, and the UAV reaches its maximum speed when x tends to 2; in the (2-x)-P plot, it is again verified that (2-x) is above 0, the oscillation curve of (2-x)-P does not lead to an oscillation curve of the t-P plot, and the overall t-P curve tends to decrease; in the w-P plot, the overall curve tends to rise because of $w = Pt$, following the law of motion.

According to Equation (9), it is known that when the variable x tends to 2, t tends to be the time when the UAV decelerates from the maximum speed to 0. Then, the weight method is able to prove that the UAV deceleration process has a time t-energy consumption w bi-objective optimal solution.

When using the weighting method to find the optimal solution for the bi-objective of UAV flight time and energy consumption, it is necessary to compare the bi-objective evaluation values of different weighting coefficients to determine the flight time weighting coefficient A and the flight energy consumption weighting coefficient B. Firstly, three sets of weighting coefficients are selected, as can be seen from the t-P and w-P images of the UAV deceleration process in Figures 18(d) and 18(e), the t-range is 14 and the w-range is 300, then the B coefficient is taken as 14/300 and the A factor is 286/300; the maximum value of t is 12.81 and the maximum value of w is 284.98, then the B factor is taken as 12.81/284.98 and the A factor is taken as 272.19/284.98; since there is no oscillation curve in the deceleration process of the UAV, i.e., there is no minimum value point, the average value of the first two coefficients is taken, then the B factor is taken as 13.405/292.49 and the A factor is taken as 279.085/292.49.

The simulation results are shown in Figures 18(f)-18(h), where (f) $z2$-P, the relationship between the bi-objective evaluation function of the first set of weighting coefficients and power; (g) $z2$-P, bi-objective evaluation function of the second set of weighting coefficients versus power; (h) $z2$-P, the bi-objective evaluation function of the third group of weighting coefficients versus power.

When the B factor is 14/300 and the A factor is 286/300, the bi-target evaluation $z2$ is 8.578; when the B factor is 13.405/292.49 and the A factor is 279.085/292.49, the bi-target evaluation $z2$ is 8.588; when the B factor is 12.81/284.98 and A factor is 272.19/284.98, the bi-target evaluation $z2$ is 8.493. By comparing the size of the bi-target evaluation $z2$, the A factor is 272.19/284.98 and B factor is 12.81/284.98 of the UAV deceleration process, and the optimal deceleration power of the UAV is 9 w. From the v-P image in Figure 18(a), it is known that the speed is 9 w when the power is 17 m/s. Meanwhile, the optimal deceleration power of the UAV to decelerate from different maximum speeds to 0 can be determined by combining Figures 18(a) and 18(h) as shown in Table 6.

5.3. **Flight integration simulation.** Combining the optimal path and flight strategy obtained by the TPA, the optimal flight strategy of the UAV on the generated optimal path can be determined based on the selection of different optimal acceleration and deceleration power. This power ensures the bi-objective optimization of the UAV's flight time and flight

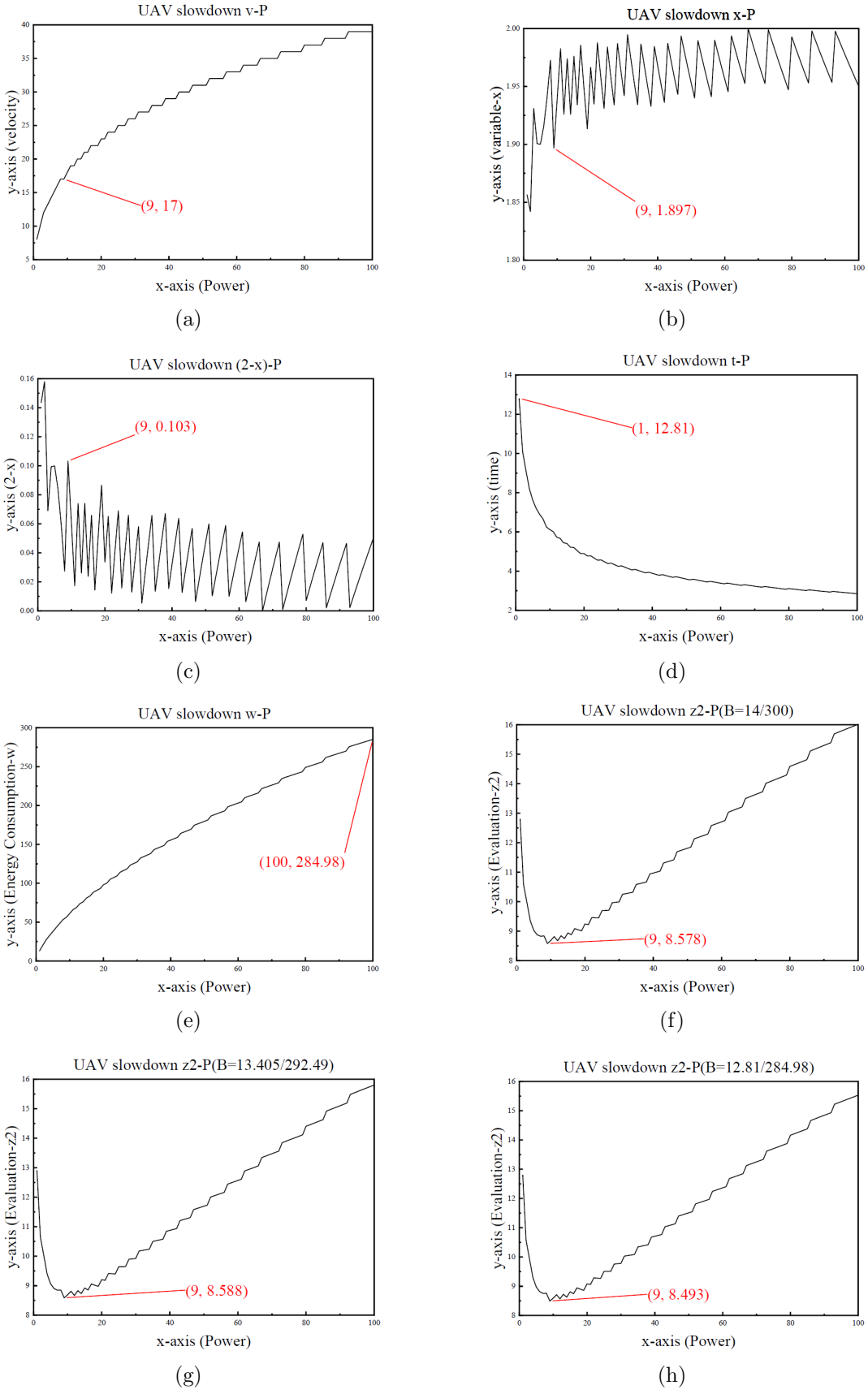

FIGURE 18. Relationship between motion parameters and bi-objective evaluation function versus power for the deceleration process of the UAV (a)-(h)

TABLE 6. Optimal deceleration power for different maximum speeds of UAV

$v_{\max}$ (m/s)	≤ 17	18	19	20
P_{sd} (w)	9	10	12	14

energy consumption. It determines the optimal flight strategy based on the information of the obstacle circles that the optimal path passes through, i.e., the two adjacent obstacle circles (including the starting and ending points) on the optimal path of the UAV are successively represented by P_i and P_{i+1}, and then the optimal flight strategy is divided into three categories.

In the first category, when $0 \leq v_i < v_{i+1}$, the radius of the obstacle circle P_{i+1} determines the speed and power, and the optimal acceleration power of the obstacle circle P_i is selected according to Table 5. The power of P_i and P_{i+1} is compared, and the optimal flight mode is decided according to the distance between the two circles. When $v_{i+1} < 11$ m/s, the optimal acceleration power of P_i is chosen to be 19 w, and the UAV has four optimal movements; when $v_{i+1} \geq 11$ m/s, the speed of P_{i+1} corresponds to the power of P_i, that is, the power of P_i and P_{i+1} is the same at this time, and the UAV has two optimal movements.

In the second category, when $v_i = v_{i+1}$, respectively, the radius of the obstacle circle P_i and P_{i+1} determines the speed and power, and the optimal acceleration/deceleration power of the obstacle circles P_i and P_{i+1} are selected according to Table 5 and Table 6. The power of P_i and P_{i+1} is compared, and the optimal flight mode is decided according to the distance between the two circles. When $v_i = v_{i+1} < 11$ m/s, the UAV has three optimal movements, with a default optimal acceleration power of 19 w and a default optimal deceleration power of 9 w; when $v_i = v_{i+1} \geq 11$ m/s, the speed of P_i and P_{i+1} corresponds to the power, and the UAV has one optimal movement, i.e., uniform motion.

In the third category, when $v_i > v_{i+1} \geq 0$, the radius of the obstacle circle P_i determines the speed and power, and the optimal deceleration power of the obstacle circle P_i is selected according to Table 6. The power of P_i and P_{i+1} is compared, and the optimal flight mode is decided according to the distance between the two circles. When $v_i < 17$ m/s, the optimal deceleration power of P_i is chosen to be 9 w, and the UAV has four optimal movements; when $v_i \geq 17$ m/s, the speed of P_i corresponds to the power, and the UAV has two optimal movements.

The paths can be generated by the TPA in six different environments. For example, the optimal flight strategy of the UAV on the optimal paths of the E6 environment is shown in Table 7.

As can be seen from Table 7, the total length of the optimal path of the UAV in the E6 environment is 725.00 m, the total flight time is 52.263 s, and the total energy consumption is 1549.92 J.

At the starting point, the UAV accelerates from 0 m/s to 14 m/s with acceleration power 31 w for 5.881 s at the distance of 59.74 m and the energy consumption of 182.31 J, and flies at a uniform speed 14 m/s with acceleration power 31 w to reach the first obstacle circle for 6.090 s at the distance of 85.26 m and the energy consumption of 188.79 J. At the first obstacle circle, the UAV flies through the circular arc at a uniform speed 14 m/s with acceleration power 34 w for 1.443 s at the distance of 16.00 m and the energy consumption of 38.86 J and begins to leave the first obstacle circle. Then the UAV flies at a uniform speed 14 m/s with acceleration power 31 w for 24.982 s at the distance of 349.74 m and the energy consumption of 774.44 J, and decelerates from 14 m/s to 12 m/s with deceleration power 9 w to reach the second obstacle circle for 0.468 s at the distance of 9.26 m and the energy consumption of 4.21 J.

TABLE 7. Optimal flight strategy for optimal path of E6 environment

Straight/Arc line		l_1	l_2	l_3	l_4	l_5	l_6	l_7
Speed-up segment	P/w	31	/	/	/	25	/	/
	t/s	5.881	/	/	/	0.842	/	/
	S/m	59.74	/	/	/	8.60	/	/
	w/J	182.31	/	/	/	21.05	/	/
Uniform segment	P/w	31	34	31	22	25	27	25
	t/s	6.090	1.143	24.982	0.667	4.569	1.462	5.591
	S/m	85.26	16.00	349.74	8.00	59.40	19.00	72.69
	w/J	188.79	38.86	774.44	14.67	114.23	39.47	139.78
	v/m/s	14	14	14	12	13	13	13
Slow-down segment	P/w	/	/	9	/	/	/	9
	t/s	/	/	0.468	/	/	/	3.568
	S/m	/	/	9.26	/	/	/	37.31
	w/J	/	/	4.21	/	/	/	32.11

At the second obstacle circle, the UAV flies through the circular arc at a uniform speed 12 m/s with acceleration power 22 w for 0.667 s at the distance of 8.00 m and the energy consumption of 14.67 J and begins to leave the second obstacle circle. Then the UAV accelerates from 12 m/s to 13 m/s with acceleration power 25 w for 0.842 s at the distance of 8.60 m and the energy consumption of 21.05 J, and flies at a uniform speed 13 m/s with acceleration power 25 w to reach the third obstacle circle for 4.569 s at the distance of 59.40 m and the energy consumption of 114.23 J. At the third obstacle circle, the UAV flies through the circular arc at a uniform speed 13 m/s with acceleration power 27 w for 1.462 s at the distance of 19.00 m and the energy consumption of 39.47 J and begins to leave the third obstacle circle. Then the UAV flies at a uniform speed 13 m/s with acceleration power 25 w for 5.591 s at the distance of 72.69 m and the energy consumption of 139.78 J, and decelerates from 13 m/s to 0 m/s with deceleration power 9 w to reach the ending point for 3.568 s at the distance of 37.31 m and the energy consumption of 32.11 J.

From Table 7, it can be obtained that the UAV has shorter flight time and less energy consumption to complete the mission on the optimal path generated in six different environments. Also, the UAV's needs can be met for multiple missions even the normal lightweight quadrotor UAV battery only stores 270 kJ of energy. The optimal path and flight strategy generated based on TPA can determine the optimal flight strategy of the UAV. The optimal acceleration and deceleration power can be determined according to the flight speed and flight time decided by the length of each sub-path. The UAV completes the mission on the optimal path with the shortest time and the most energy-efficient optimal flight strategy. Therefore, the UAV can effectively avoid obstacles and have the optimal flight index perform the mission and return.

6. **Conclusions.** In order to effectively plan collision-free paths in a static environment, this paper proposes an optimal path planning algorithm TPA based on the viewable tangent point method. Buildings as obstacles are reconstructed into two-dimensional circles on the map. The straight-line segments between the tangent points of the two circles near the start-end line are used as sub-paths, and the arcs between the tangent points on the same obstacle circle are used as smooth curves to connect different straight-line

segments. Then the total path length of different sub-path combinations is traversed and compared to obtain the satisfactory collision-free optimal path. The optimal power and flight strategy on the selected path are determined by the UAV kinematic model, so as to ensure the bi-objective optimization of flight time and flight energy consumption. The effectiveness of TPA is verified through a large number of computing experiments, and the following conclusions are drawn.

Firstly, the TPA can generate satisfactory collision-free paths with the shortest computing time in six static environments. Especially, the TPA just consumes 0.1 seconds under different instances with dense obstacles, which is far less than the time consumption of other compared algorithms. Secondly, the acceleration process and deceleration process of UAV kinematics are simulated to determine the optimal acceleration and deceleration power of the UAV. Finally, the optimal path, flight strategy and optimal power are integrated, and the optimal flight strategy is determined by numerical simulation in six environments to ensure the bi-objective optimization of flying time and energy consumption.

However, the limitations of the TPA are mainly reflected in the following aspects. It is a deterministic algorithm that generates a collision-free path based on a specific mathematical formulation. Dynamic obstacles encountered are not currently considered in static environments. TPA does not consider optimal path planning in unknown environment.

Therefore, the application of the TPA to a quadrotor UAV will be considered to further verify the simulation results in this paper in the future. Future research will focus on UAV automatic obstacle avoidance and path planning methods in unknown environments.

REFERENCES

[1] J. Liu, X. Qin, B. Qi and X. Cui, 3D online path planning of UAV based on improved differential evolution and model predictive control, *International Journal of Innovative Computing, Information and Control*, vol.16, no.1, pp.315-329, 2020.

[2] Z. Wang, P. Yang, X. Hu, Z. Zhang and C. Wen, Sliding mode fault tolerant control of quadrotor UAV with state constraints under actuator fault, *International Journal of Innovative Computing, Information and Control*, vol.17, no.2, pp.639-653, 2021.

[3] Y. Zheng, Q. Yang, H. Ren, D. Wang, C. Zhao and W. Zhao, Spatial pattern variation of artificial sand-binding vegetation based on UAV imagery and its influencing factors in an oasis-desert transitional zone, *Ecological Indicators*, vol.141, 2022.

[4] X. Liu and N. Ansari, Resource allocation in UAV-assisted M2M communications for disaster rescue, *IEEE Wireless Communications Letters*, vol.8, no.2, pp.580-583, 2019.

[5] D. Erdi, B. Rajan, K. Murat and T. O. Diclehan, UAV routing for reconnaissance mission: A multi-objective orienteering problem with time-dependent prizes and multiple connections, *Computers and Operations Research*, vol.145, 2022.

[6] X. Liang, Z. Zhang, H. Yu, Y. Wang, Y. Fang and J. Han, Antiswing control for aerial transportation of the suspended cargo by dual quadrotor UAVs, *IEEE/ASME Transactions on Mechatronics*, vol.27, no.6, pp.5159-5172, 2022.

[7] B. Zhu, C. Li, L. Song, Y. Song and Y. Li, A* algorithm of global path planning based on the grid map and V-graph environmental model for the mobile robot, *2017 Chinese Automation Congress (CAC)*, Jinan, China, pp.4973-4977, 2017.

[8] Z. Zhou, J. Wang, Z. Zhu, D. Yang and J. Wu, Tangent navigated robot path planning strategy using particle swarm optimized artificial potential field, *Optik*, vol.158, pp.639-651, 2018.

[9] D. František, B. Andrej, K. Martin, B. Peter, F. Martin, F. Tomas and J. Ladislav, Path planning with modified A star algorithm for a mobile robot, *Procedia Engineering*, vol.96, pp.59-69, 2014.

[10] S. Sedighi, D.-V. Nguyen and K.-D. Kuhnert, Guided hybrid A-star path planning algorithm for valet parking applications, *2019 5th International Conference on Control, Automation and Robotics (ICCAR)*, Beijing, China, pp.570-575, 2019.

[11] H. Chen, K. Chang and C. S. Agate, UAV path planning with tangent-plus-Lyapunov vector field guidance and obstacle avoidance, *IEEE Transactions on Aerospace and Electronic Systems*, vol.49, no.2, pp.840-856, 2013.

[12] Y. Wang, H. Wang and Y. Lun, Shortest path planning of UAV for target tracking and obstacle avoidance in 3D environment, *2020 39th Chinese Control Conference (CCC)*, Shenyang, China, pp.3385-3390, 2020.

[13] A. Rashid, A. Marhoon and Z. Yahia, An algorithm for path planning with polygon obstacles avoidance based on the virtual circle tangents, *Journal of Electrical and Electronic Engineering (EEEJ)*, vol.12, pp.221-234, 2016.

[14] L. P. Tomás and A. W. Michael, An algorithm for planning collision-free paths among polyhedral obstacles, *Communications of the ACM*, vol.22, pp.560-570, 1979.

[15] A. B. Doyle and D. I. Jones, A tangent based method for robot path planning, *Proc. of the 1994 IEEE International Conference on Robotics and Automation*, San Diego, CA, USA, vol.2, pp.1561-1566, 1994.

[16] H. Liu, X. Li, M. Fan, G. Wu, W. Pedrycz and P. N. Suganthan, An autonomous path planning method for unmanned aerial vehicle based on a tangent intersection and target guidance strategy, *IEEE Transactions on Intelligent Transportation Systems*, vol.23, no.4, pp.3061-3073, 2022.

[17] S. Ossyra, Z. Chen, R. J. Lee, A. Ahmad, R. Pham, K. Fenstermacher and S. Bhandari, Tangent-based method for collision detection and avoidance system for UAVs using ADS-B transponder and ADS-B like solution, *2022 International Conference on Unmanned Aircraft Systems (ICUAS)*, Dubrovnik, Croatia, pp.1571-1579, 2022.

[18] R. Bohlin and L. E. Kavraki, Path planning using lazy PRM, *Proceedings 2000 ICRA. Millennium Conference. IEEE International Conference on Robotics and Automation. Symposia Proceedings (Cat. No. 00CH37065)*, San Francisco, CA, USA, vol.1, pp.521-528, 2000.

[19] G. Sánchez and J. C. Latombe, On delaying collision checking in PRM planning: Application to multi-robot coordination, *The International Journal of Robotics Research*, vol.21, no.1, pp.5-26, 2002.

[20] S. Li, A. Yang and L. Chen, Path planning algorithm on large scale terrain data based on PRM with non-uniform sampling strategy, *2021 IEEE 2nd International Conference on Information Technology, Big Data and Artificial Intelligence (ICIBA)*, Chongqing, China, vol.2, pp.203-207, 2021.

[21] M. Huppi, L. Bartolomei, R. Mascaro and M. Chli, T-PRM: Temporal probabilistic roadmap for path planning in dynamic environments, *IEEE/RSJ International Conference on Intelligent Robots and Systems (IROS)*, Tokyo, Japan, 2022.

[22] B. Uzun, H. Gozde and M. C. Taplamacioglu, Hybrid operation of A* and PRM algorithms for efficient path planning in autonomous mobile robots, *International Journal on Technical and Physical Problems of Engineering*, vol.14, no.28, pp.183-189, 2022.

[23] J. J. Kuffner and S. M. LaValle, RRT-connect: An efficient approach to single-query path planning, *Proceedings 2000 ICRA. Millennium Conference. Ieee International Conference on Robotics and Automation. Symposia Proceedings (Cat. No. 00CH37065)*, San Francisco, CA, USA, vol.2, pp.995-1001, 2000.

[24] J. D. Gammell, S. S. Srinivasa and T. D. Barfoot, Informed RRT*: Optimal sampling-based path planning focused via direct sampling of an admissible ellipsoidal heuristic, *2014 IEEE/RSJ International Conference on Intelligent Robots and Systems*, Chicago, IL, USA, pp.2997-3004, 2014.

[25] Z. Tahir, A. H. Qureshi, Y. Ayaz and R. Nawaz, Potentially guided bidirectionalized RRT* for fast optimal path planning in cluttered environments, *Robotics and Autonomous Systems*, vol.108, pp.13-27, 2018.

[26] H. Zhang, Y. Wang, J. Zheng and J. Yu, Path planning of industrial robot based on improved RRT algorithm in complex environments, *IEEE Access*, vol.6, pp.53296-53306, 2018.

[27] Y. Li, W. Wei, Y. Gao, D. Wang and Z. Fan, PQ-RRT*: An improved path planning algorithm for mobile robots, *Expert Systems with Applications*, vol.152, 2020.

[28] J. Wang, W. Chi, C. Li, C. Wang and M. Q.-H. Meng, Neural RRT*: Learning-based optimal path planning, *IEEE Transactions on Automation Science and Engineering*, vol.17, no.4, pp.1748-1758, 2020.

[29] J. Qi, H. Yang and H. Sun, MOD-RRT*: A sampling-based algorithm for robot path planning in dynamic environment, *IEEE Transactions on Industrial Electronics (TIE)*, vol.68, no.8, pp.7244-7251, 2021.

[30] X. Zhang, S. Xia, X. Li and T. Zhang, Multi-objective particle swarm optimization with multi-mode collaboration based on reinforcement learning for path planning of unmanned air vehicles, *Knowledge-Based Systems*, vol.250, 2022.

[31] V. Roberge, M. Tarbouchi and G. Labonté, Comparison of parallel genetic algorithm and particle swarm optimization for real-time UAV path planning, *IEEE Transactions on Industrial Informatics*, vol.9, no.1, pp.132-141, 2013.
[32] J. Chen, F. Ling, Y. Zhang, T. You, Y. Liu and X. Du, Coverage path planning of heterogeneous unmanned aerial vehicles based on ant colony system, *Swarm and Evolutionary Computation*, vol.69, 2022.
[33] Y. Zhao, Z. Zheng, X. Zhang and Y. Liu, Q learning algorithm based UAV path learning and obstacle avoidence approach, *2017 36th Chinese Control Conference (CCC)*, Dalian, China, pp.3397-3402, 2017.
[34] T. I. Zohdi, The game of drones: Rapid agent-based machine-learning models for multi-UAV path planning, *Computational Mechanics*, vol.65, pp.217-228, 2019.
[35] V. Sathiya, M. Chinnadurai and S. Ramabalan, Mobile robot path planning using fuzzy enhanced improved multi-objective particle swarm optimization (FIMOPSO), *Expert Systems with Applications*, vol.198, 2022.
[36] Y. V. Pehlivanoglu and P. Pehlivanoglu, An enhanced genetic algorithm for path planning of autonomous UAV in target coverage problems, *Applied Soft Computing*, vol.112, 2021.
[37] M. Shafiq, Z. A. Ali, A. Israr, E. H. Alkhammash, M. Hadjouni and J. J. Jussila, Convergence analysis of path planning of multi-UAVs using max-min ant colony optimization approach, *Sensors*, vol.22, no.14, 5395, 2022.
[38] L. Yang, J. Guo and Y. Liu, Three-dimensional UAV cooperative path planning based on the MP-CGWO algorithm, *International Journal of Innovative Computing, Information and Control*, vol.16, no.3, pp.991-1006, 2020.

Author Biography

Yuanlong Yue received the B.Sc. degree in automation and the Ph.D. degree in control science and engineering from China University of Petroleum (Beijing), China, in 2008 and 2014, respectively.

He is currently a senior engineer in automation at the College of Information Science and Engineering, China University of Petroleum (Beijing), China. His research interests include subsea communication protocol, highly reliable imbedded system design, and multi-sensor data fusion. He is the author or coauthor of more than 20 refereed technical papers, and he is the holder of 6 patents in his areas of interest.

Daifeng Zhang obtained his Bachelor degree in automation from China University of Petroleum (Beijing), China in 2020 and he is currently working toward the M.Sc. degree in control science and engineering at China University of Petroleum (Beijing).

He has written two invention-type patents and a project thesis during his master's degree, and has won the first prize in the school-level academic award for three consecutive years and the first prize in the school-level innovation and entrepreneurship competition. His research interests are mainly focused on UAV path optimization, tracking control and cluster control.

Lvyin Niu obtained his Bachelor degree in automation from China University of Petroleum (Beijing), China in 2020 and he is currently working toward the M.Sc. degree in control science and engineering at China University of Petroleum (Beijing).

He is good at computer programming in various languages. He participated in the development of operational research teaching software, industrial process host computer operating system and Modbus RTU master during his undergraduate and graduate studies. The current research direction focuses on UAV dynamic obstacle avoidance and real-time path planning.

Xin Zuo received the B.Sc. degree from East China Petroleum Institute (now China University of Petroleum (Beijing)), China, in 1984; he worked as the assistant at East China Petroleum Institute from September 1984 to August 1987; he received the Master degree in China University of Petroleum (Beijing), China, in 1990.

He is currently a full-time professor at the College of Information Science and Engineering, China University of Petroleum (Beijing), China. He is a member of Expert Committee of China National Association for Automation in Petroleum and Chemical Industry. He is the author or coauthor of more than 110 refereed technical papers, and he is the holder of 20 patents in his areas of interest. His research interests include subsea production control systems design, subsea production reliability research, process control design and real-time optimization.